AD-A040 437 PHYSICAL SCIENCES INC WOBURN MASS F/G 20/5
RADIATION-INDUCED SOUND.(U)
JAN 77 P E NEBOLSINE N00014-76-C-0693
UNCLASSIFIED PSI-TR-82 NL

| OF |
AD
A040437

END

DATE
FILMED
6-77

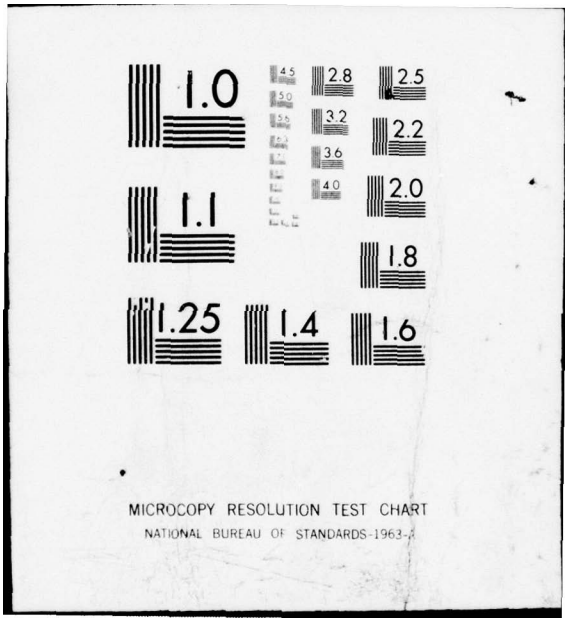
1.0
1.1
1.25
1.4
1.6
1.8
2.0
2.2
2.5
2.8
3.2
3.6
4.0
4.5
5.0
5.6
MICROCOPY RESOLUTION TEST CHART
NATIONAL BUREAU OF STANDARDS-1963-A

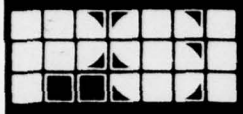

RADIATION-INDUCED SOUND

FINAL REPORT

by

P. E. Nebolsine

January 1977

Sponsored by

OFFICE OF NAVAL RESEARCH
Department of the Navy
Arlington, VA 22217

Contract No. N00014-76-C-0693

NR 261-206

PHYSICAL SCIENCES INC.
30 COMMERCE WAY, WOBURN, MASS. 01801

UNCLASSIFIED

SECURITY CLASSIFICATION OF THIS PAGE (When Data Entered)

REPORT DOCUMENTATION PAGE

READ INSTRUCTIONS BEFORE COMPLETING FORM

1. REPORT NUMBER

2. GOVT ACCESSION NO.

3. RECIPIENT'S CATALOG NUMBER

4. TITLE (and Subtitle)
RADIATION-INDUCED SOUND

5. TYPE OF REPORT & PERIOD COVERED
FINAL REPORT
3/15/76 - 12/30/76

6. PERFORMING ORG. REPORT NUMBER
PSI-TR-82

7. AUTHOR(s)
P. E. Nebolsine

8. CONTRACT OR GRANT NUMBER(s)
N00014-76-C-0693 new

9. PERFORMING ORGANIZATION NAME AND ADDRESS
Physical Sciences Inc.
30 Commerce Way
Woburn, MA 01801

10. PROGRAM ELEMENT, PROJECT, TASK AREA & WORK UNIT NUMBERS

11. CONTROLLING OFFICE NAME AND ADDRESS
Office of Naval Research
Department of the Navy
Arlington, VA 22217

12. REPORT DATE
January 1977

13. NUMBER OF PAGES
69

14. MONITORING AGENCY NAME & ADDRESS(if different from Controlling Office)
Final rept.
15 Mar - 30 Dec 76,

15. SECURITY CLASS. (of this report)
Unclassified

15a. DECLASSIFICATION/DOWNGRADING SCHEDULE

16. DISTRIBUTION STATEMENT (of this Report)
Distribution "Unlimited"
12 71p.

17. DISTRIBUTION STATEMENT (of the abstract entered in Block 20, if different from Report)

18. SUPPLEMENTARY NOTES

19. KEY WORDS (Continue on reverse side if necessary and identify by block number)
Laser
Acoustics
Blast Wave
Propagation
Fluid Mechanics

micrometer

20. ABSTRACT (Continue on reverse side if necessary and identify by block number)

Radiation-induced-sound experiments were conducted with one to four 10.6 μ CO_2 laser pulses. These experiments were conducted to demonstrate the ability to control the acoustic energy spectral density. The acoustic signatures were Fourier analyzed to obtain the energy spectral density. The results show that the ratio of the width of a peak in the spectrum to the fundamental frequency scales approximately as the → next pg

DD FORM 1 JAN 73 1473 EDITION OF 1 NOV 65 IS OBSOLETE

UNCLASSIFIED

SECURITY CLASSIFICATION OF THIS PAGE (When Data Entered)

391 105

AB

inverse of the number of pulses. This scaling does not hold if the pulses are not evenly spaced or not even in amplitude.

Theoretical modeling formulated scaling laws relating laser parameters to acoustic parameters of the generated signatures. Theoretical predictions were also made of the change in amplitude and shape of the broadband signals due to frequency-dependent absorption as a function of propagation distance.

ABSTRACT

Radiation induced sound experiments were conducted with one to four 10.6μ CO_2 laser pulses. These experiments were conducted to demonstrate the ability to control the acoustic energy spectral density. The acousic signatures were Fourier analyzed to obtain the energy spectral density. The results show that the ratio of the width of a peak in the spectrum to the fundamental frequency scales approximately as the inverse of the number of pulses. This scaling does not hold if the pulses are not evenly spaced or not uniform in amplitude.

Theoretical modeling formulated scaling laws relating laser parameters to acoustic parameters of the generated signatures. Theoretical predictions were also made of the change in amplitude and shape of the broadband signals due to frequency-dependent absorption as a function of propagation distance.

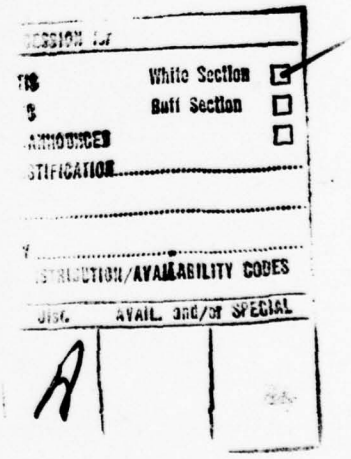

ACKNOWLEDGEMENTS

The author would like to acknowledge the assistance of Paul Kingston and Edward McCracken in performing the experiments and of John Cronin for his computer programing which was used in the data reduction process. The author would also like to acknowledge many useful discussions with Drs. Robert Weiss, Kurt Wray, and Peter Wu and to thank Ms. I. Scanzillo for typing this report.

TABLE OF CONTENTS

I. INTRODUCTION

The physics of radiation induced sound has previously been investigated both theoretically and experimentally[1-9], but past experiments have been concerned with single pulses only[1-5,8]. In this report we discuss theoretical and experimental results with one to four laser induced acoustic pulses and the resultant pulse train.

A major criticism of prior radiation induced sound experiments was that the source bandwidth was too great to be useful. Therefore, this experimental program was undertaken to demonstrate that narrower-band sound could be generated with multiple laser pulses. The most flexible and cost effective approach was to simulate only the first four pulses of a long pulse train with a laser system consisting of four independently triggered lasers. This laser system was assembled from four CO_2 laser kits and one power supply. The experiments are discussed in Section III. The experimental results demonstrate that the bandwidth can be controlled by the number of laser induced acoustic pulses.

The theoretical effort, reported on in Section II, was an extension of previous work. The earlier analysis, which was done for PMS-405 of the Naval Sea Systems Command, established the basic scaling laws of 3D blast wave induced sound.[7] This work was recently extended and modified to predict theoretically the far-field acoustic amplitude as a function of time.[9] The far-field signature is predicted from linear acoustics, and the predictions were made to estimate the change in the signature due to the frequency dependent absorption coefficient of water. No dispersion of sound waves is used or appears to have been observed, but a broadband signature does spread out in time.[4] This spreading is due to the approximately quadratic dependence of the absorption coefficient on frequency:

for a fixed propagation distance the high-frequency components making up the broad band signature are attenuated more than the low-frequency components. It is well known from Fourier analysis that a waveform may spread in time as its spectrum is reduced in width.

Conclusions and suggestions for future work are discussed in Section IV.

II. THEORY

Past theoretical work on radiation-induced sound treated the phenomenology in two limits. First, the steady-state coupling problem was analyzed.[6] This work yielded the conclusion that an induced surface pressure, p_s, would be proportional to the laser-beam irradiance, I_o:

$$p_s = C I_o \quad , \tag{2.1}$$

where C, the ratio of the pressure to the irradiance, is commonly called the coupling coefficient. The work done by Pirri yielded $C \cong 25$ dyne/W for $10^5 < I_o < 10^7$ W/cm^2.[6] In the second limit of the phenomenology, it was assumed that a steady-state situation would not occur, and that blast-wave theory would be most appropriate to use.[7,9] The application of blast-wave theory to analyze the radiation-induced-sound phenomenology is a method to uncouple the optical radiation from the fluid mechanics of the water and water vapor. In the model, a short-pulse laser beam-pulse laser beam irradiates water with a fluence much greater than the threshold fluence. The threshold fluence E_T is defined as the energy per unit area sufficient to "boil" an infinitesimal layer of water and is a function of the optical depth and the properties of water. This calculated energy must be delivered in a time short enough so that heat conduction is insignificant. The calculated values of E_T are reproduced from Ref. 9 in Table I for various laser wavelengths. We were experimentally restricted to 10.6 μ radiation, for which the threshold fluence is 3 J/cm^2. When the laser fluence is much greater than the threshold fluence, a small amount of water is raised to a temperature and pressure high in comparison with the normal boiling conditions of 100°C and 10^6 dynes/cm^2. The water vapor drives a shock wave away from the irradiated

TABLE I

THRESHOLD FLUENCE FOR VARIOUS LASER LINES

Laser	Lines	Laser Wavelength μm	Threshold Fluence J/cm^2
CO_2	P (20)	10.6	3
CO	8-7 Band P (14)	5.25	11
	9-8 Band P (10)	5.27	11
DF	2-1 Band P (6)	3.73	14
	2-1 Band P (8)	3.80	14
	2-1 Band P (9)	3.84	14
HF	2-1 Band P (7)	2.87	0.2
	2-1 Band P (8)	2.91	0.2

area. We assume that for the duration of the blast wave, i.e., for tens of microseconds, the behavior is dominated by the blast-wave solution in air and that the water surface is unperturbed. Sensible displacements of the water occur tens of milliseconds after the radiation pulse.

Blast-wave theory assumes an instaneous release of energy with n omass addition. In our case there can be significant mass addition, but it will be ignored to keep the problem tractable. Recently, blast-wave theory has been extended to include a noninstantaneous release of energy.[10] We use this formulation while the laser pulse is on, and then match the solutions of classical blast wave theory to the variable energy theory at the pulse "off" time.

We consider a constant-input-power case; the power can be deposited in a plane for 1D expansions, in a line for 2D expansions, and at a point for 3D expansions. The shock radius and pressure are used to model the radiation-induced sound source. Variable-blast-wave theory yields a solution for the shock radius R_s, which is:[10]

$$R_s = Kt^{3/(\alpha + 3)} , \tag{2.2}$$

where

$$K = \left(\frac{I a_o^2}{p_o \left(\frac{3}{\alpha + 3} \right)^2 J_o} \right)^{1/(\alpha + 3)}$$

and

J_o is a constant with values 1, .57 and .4 , nd

α = 0, 1, 2 for 1D, 2D, and 3D expansions, respectively.

a_o is the sound speed in air ,

p_o is the ambient pressure ,

I is the input power per unit area for $\alpha = 0$,

I is the input power per unit length/2π for $\alpha = 1$, and

I is the input power / 4π for $\alpha = 2$.

t is time measured from the start of the energy release (i.e. from the time at which the accumulated laser-applied energy per unit area equals the threshold fluence) and limited its value, τ, at the end of the laser pulse. The shock pressure, p, is given by:

$$p = \frac{2}{\gamma + 1} \rho_o \left(\frac{dR_s}{dt} \right)^2 \quad , \tag{2.3}$$

where Eq. (2.2) is used for R_s and γ is the ratio of specific heats. The early time solution will be one dimensional. In this case we have:

$$p = \frac{2}{\gamma + 1} \rho_o \left(\frac{I a_o^2}{p_o} \right)^{2/3} \quad . \tag{2.4}$$

The surface pressure for the 1D case, P_{1D}, is approximately one half the shock pressure because the pressure behind the shock front falls off steeply to a value approximately one half the value given by Eq. (2.4). Thus we have

$$p_{1D} = \frac{1}{\gamma + 1} \rho_o \left(\frac{I a_o^2}{p_o} \right)^{2/3} \qquad 0 \leq t \leq \tau \ . \tag{2.5}$$

By numerical computation with Eq. (2.2) and an input power per unit area of 10^8 W/cm^2 the shock radius will have grown to 1 cm in 1 μsec. Because the spot sizes which were experimentally used were approximately 1 x 2 cm, 1D variable-energy blast-wave theory is appropriate to use during at least the first part of the laser pulse duration. However, after the laser

pulse if off the expansion is three dimensional, because the shock radius has grown to be larger than the spot dimension. In what follows, the approximation has been made that one-dimensional blast-wave theory is appropriate during the whole duration of the laser pulse and that 3-dimensional blast-wave behavior occurs immediately thereafter.

Figure 2.1 is a plot of the surface pressure versus I, the available power per unit area. These values will be used in the computation of a far-field acoustic signature. Experimental measurements have demonstrated clean-air breakdown levels of greater than 10^9 W/cm^2 for 10.6 μ radiation. Dirty-air breakdown levels with a 10.6 μ laser wavelength range from 10^7 to 10^9 W/cm^2 for particles ranging from 30 to 1 μ diameter for a 1 μsec pulse,[11] and an air/water breakdown threshold of 10^8 W/cm^2 with 10.6 μ laser wavelength has been measured.[2]

Blast-wave theory requires specification of the power or energy deposited in the gas. An approximate method to relate the laser energy to the blast-wave energy per unit area is to subtract from the pulse duration a time sufficient for the deposition of the threshold fluence. After the laser pulse is off, the blast wave will decay according to the 3D blast-wave theory discussed above. The shock radius, R_s, is given by

$$R_s = R_1 \left(\frac{t}{\tau}\right)^{2/5} , \tag{2.6}$$

where R_1 is taken to be the shock radius at the end of the laser pulse which has a pulse time τ; R_1 can be evaluated from Eq. (2.2). The surface pressure, p_s, scales according to

$$p_s = p(\tau) \left(\frac{t}{\tau}\right)^{-6/5} , \tag{2.7}$$

where $p(\tau)$ is the pressure at time τ. We match the 1D and 3D pressures at this time, and find that

$$p_s = p_{1D} (t/\tau)^{-6/5} . \tag{2.8}$$

The above information will now be used to compute an acoustic signature.

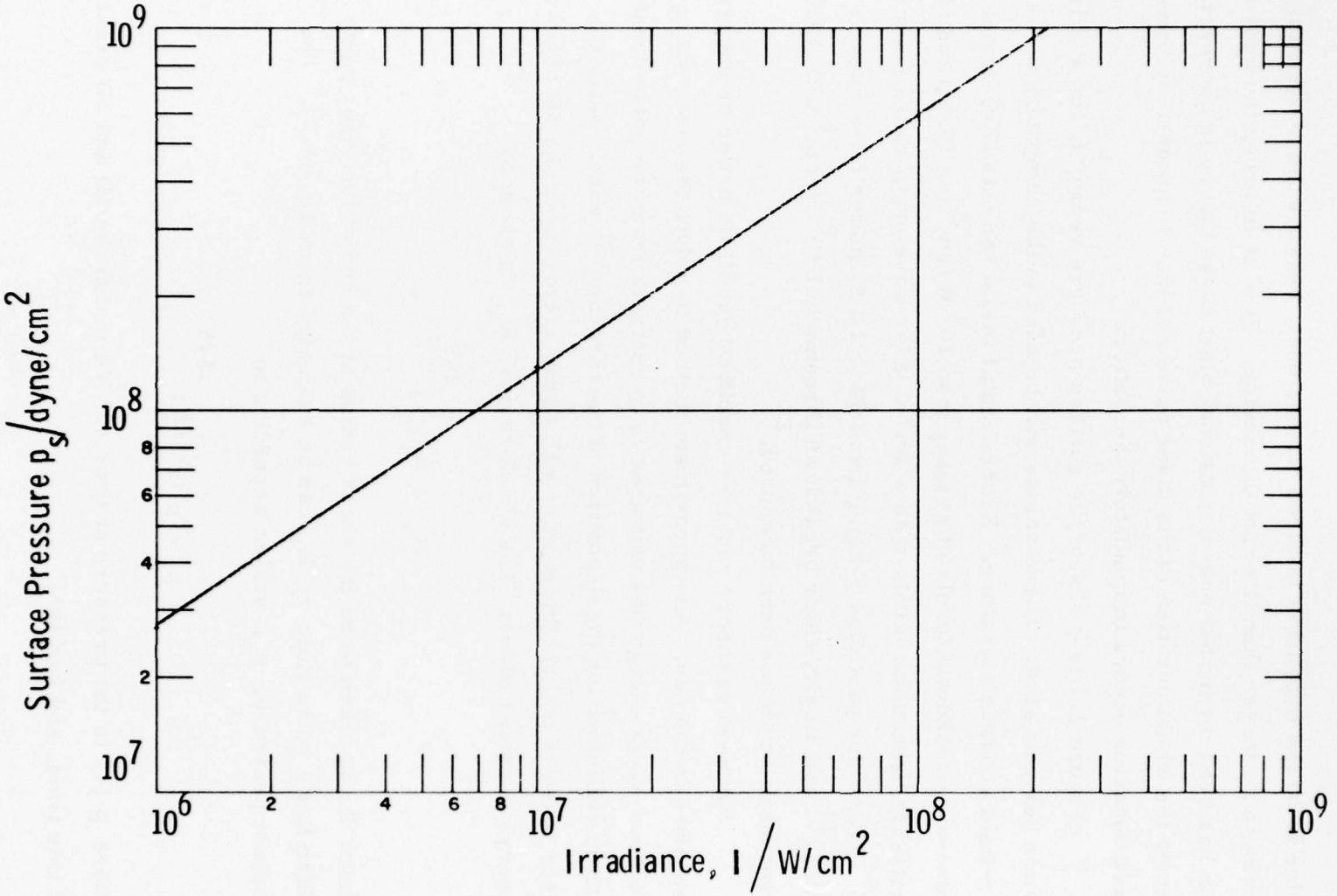

Fig. 2.1-1D Surface Pressure versus Irradiance

The well known formula for a broadband acoustic signature, $p\left(r,\ t + \frac{r}{a}\right)$, measured at a point normal to the source is:

$$p\left(r,\ t + \frac{r}{a}\right) = \frac{1}{2\pi r a} \frac{\partial}{\partial t} \int_A p_s \, dA \ , \tag{2.9}$$

where a is the sound speed in water and the notation indicates an area integration over the water surface.

Equation (2.9) will be solved by inserting Eqs. (2.5) and (2.8), the assumption that the surface pressure is constant over an area A_o of the water surface and zero elsewhere will be used to simplify the integrals. Thus we have:

$$p\left(r,\ t + \frac{r}{a}\right) = \frac{1}{2\pi r a} A_o \left\{ \frac{\rho_o}{\gamma + 1} \left(\frac{I a_o^2}{p_o} \right)^{2/3} \delta\left(t + \frac{r}{a}\right) \right\} \qquad 0 < t < \tau \tag{2.10}$$

$$p\left(r,\ t + \frac{r}{a}\right) = -\left(\frac{2}{5}\right) \frac{1}{2\pi r a} \pi R_1^2 \frac{P_{1D}\, \tau^{2/5}}{t^{7/5}} \qquad t \geq \tau, \tag{2.11}$$

where the approximation has been made that while the laser pulse is on, the area A_o is the laser beam area. After the laser pulse is off, the 3D expansion of the shock is used over the water. We note that the problem for a solely 3D expansion has already been treated.[7] The approximation which "matches" the blast-wave behavior during the time when the laser pulse is on to the subsequent behavior (when the laser pulse is off), requires the assumption that πR_1^2 in Eq. (2.11) is equal to A_o in Eq. (2.10). A more exact treatment is beyond the scope of this work.

At this point it is appropriate to consider the validity of Eq. (2.9), which assumes that, in the water, linear acoustics is applicable. From the bulk compressibility modulus of water (2×10^{10} dyne/cm^2) -- an overpressure of 10^9 dynes/cm^2 would be required to generate a density change of 5%. Thus it would appear Eq. (2.11) is valid as long as the pressure is below 10^9 dynes/cm^2. We shall see that this criterion is met for our experiments.

We note that for a fixed pulse time τ, the time for the signature to decay to any given fraction of its greatest amplitude is independent of energy. Therefore, only the magnitude of the energy spectral density will change, and not the peak frequency or other aspect of spectral shape. This conclusion is valid only within the context of our idealized model. In fact, a blast wave with counterpressure will yield an energy spectral density changing in magnitude and shape as a function of energy. However, the solution of the blast wave problem with counterpressure must be treated numerically, and we will restrict our attention to the analytic solutions of blast waves without counterpressure even though certain anomalies in the resulting solution could be developed there from.

A graphical representation of the far-field term of Eq. (2.11) is useful for making predictions of the far-field acoustic amplitude. We assume a 1-μsec laser pulse and 1-cm^2 laser beam area and evaluate the far-field amplitude at t = 1μsec, t = 5μsec, and t = 10μsec for r = 1 m. The results are shown in Fig. 2.2 where the rare faction amplitude is plotted versus irradiance. As noted above, the threshold fluence is 3 J/cm^2, and the plot cannot be used below 3×10^6 W/cm^2 if τ is 1μsec. The hydrophone may be considered to be in the far field if its distance from the dipole source is greater than one wavelength of sound for each frequency of interest. This criterion is met for frequencies greater than 1500 Hz. Therefore, for measurement depths of 1 m there is no doubt that the data is far field for our broadband signatures.

The predictions of the propagation characteristics of the generated acoustic pulses is a nontrivial problem. An approximate method will be used to predict the signature for a propagation path for which absorption

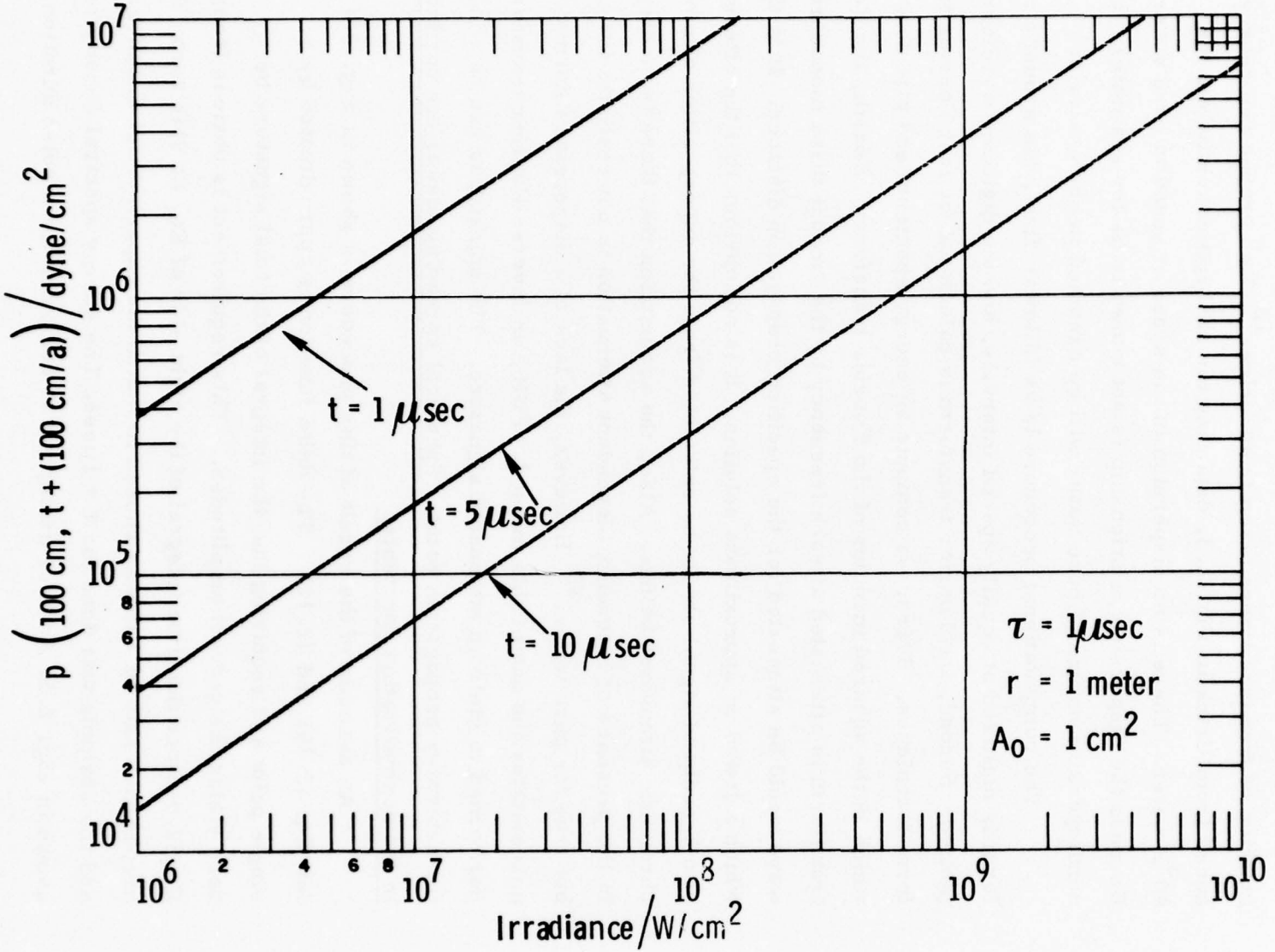

Fig. 2.2 Rarefaction Amplitude versus Irradiance

is dominant. The equations describing the absorption coefficient as a function of frequency were taken from Urick.[12] Two graphs are reproduced from Urick in Fig. 2.3, depicting the absorption coefficient for 40°F water. There is no dispersion in the speed of sound in pure water.[13] Because the dispersion relationship is not known to us for sea water, the nondispersive nature of pure water will be assumed in our analysis.

The computational procedure is as follows: first, the acoustic wave form is digitized at equally spaced intervals, and the digitized waveform is plotted. Second, the Fourier transform is calculated by fast Fourier transform techniques. Third, we compute an energy spectrum and plot density, which is the squared modulus of the Fourier transform. Fourth, the Fourier transform is attenuated at each frequency by the amount that a monochromatic wave would be attenuated for the specified propagation distance. It is this step which allowed an approximate solution. It is not obvious that the attenuation of a broadband signal should be calculated from the superposition of monochromatic attenuated values. Also, the assumption that there is no dispersion in the presence of frequency-dependent attenuation is not realistic for sea water but true for pure water.[13] However, the lack of a dispersion information necessitates the use of this method. Fifth, an inverse Fourier transform is performed to yield an attenuated signature. The signatures can be computed for arbitrary propagation paths. Spherical spreading losses are not included in the normalization constants.

An example of the result of this procedure is shown in Fig. 2.4 for Eq. (2.10) and (2.11). The delta function is approximated by a single point and requiring that the integral of the total signature be zero yields the correct amplitudes. This requirement is obvious from Eq. (2.9) since the time integral of the right side of Eq. (2.9) is zero. The propagation path of 1 m was chosen to match the experimental distance, and the example was done for $\tau = 1\mu$sec. The energy spectral density is shown in Fig. 2.5. Another example was computed for a pulse duration of

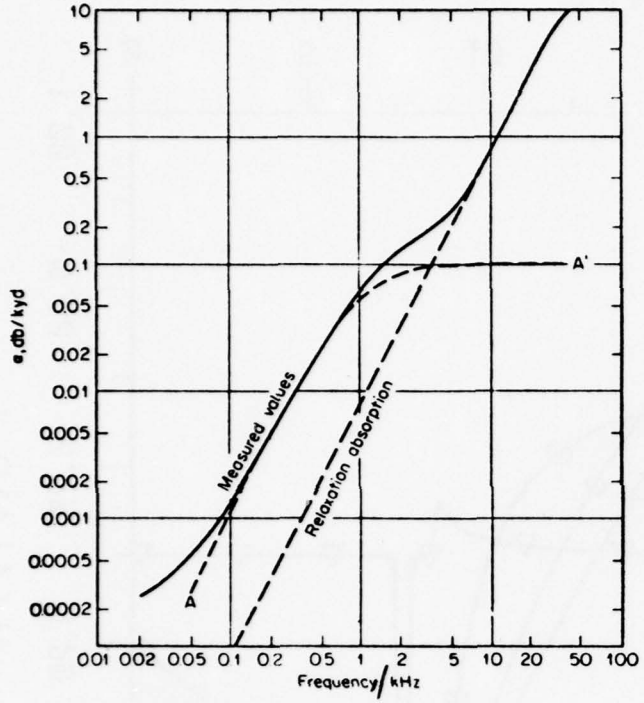

Low-frequency attenuation coefficients. [Solid curve is the center of measured data compiled by Thorp (16).]

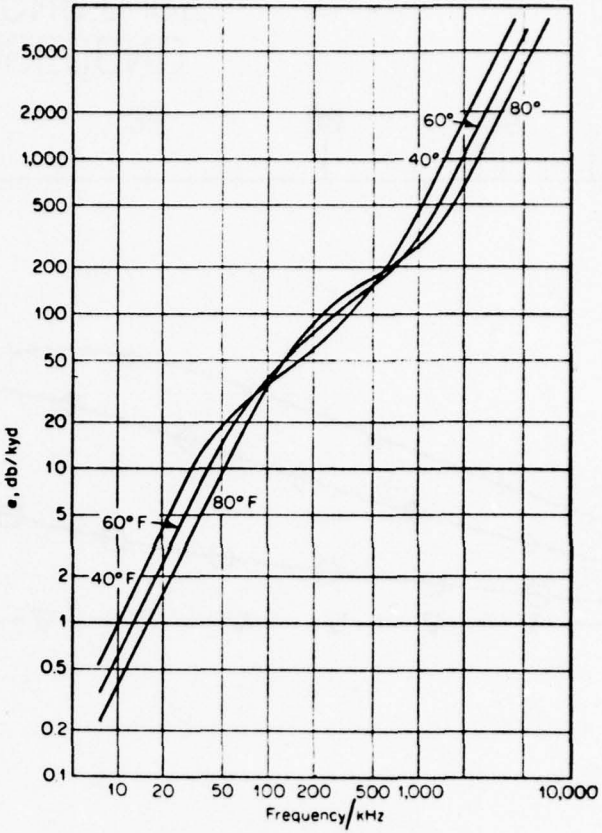

Absorption coefficient in seawater of salinity 35 ppt as a function of frequency at three temperatures.

Fig. 2.3 Absorption Coefficients versus Frequency from Urick[12]

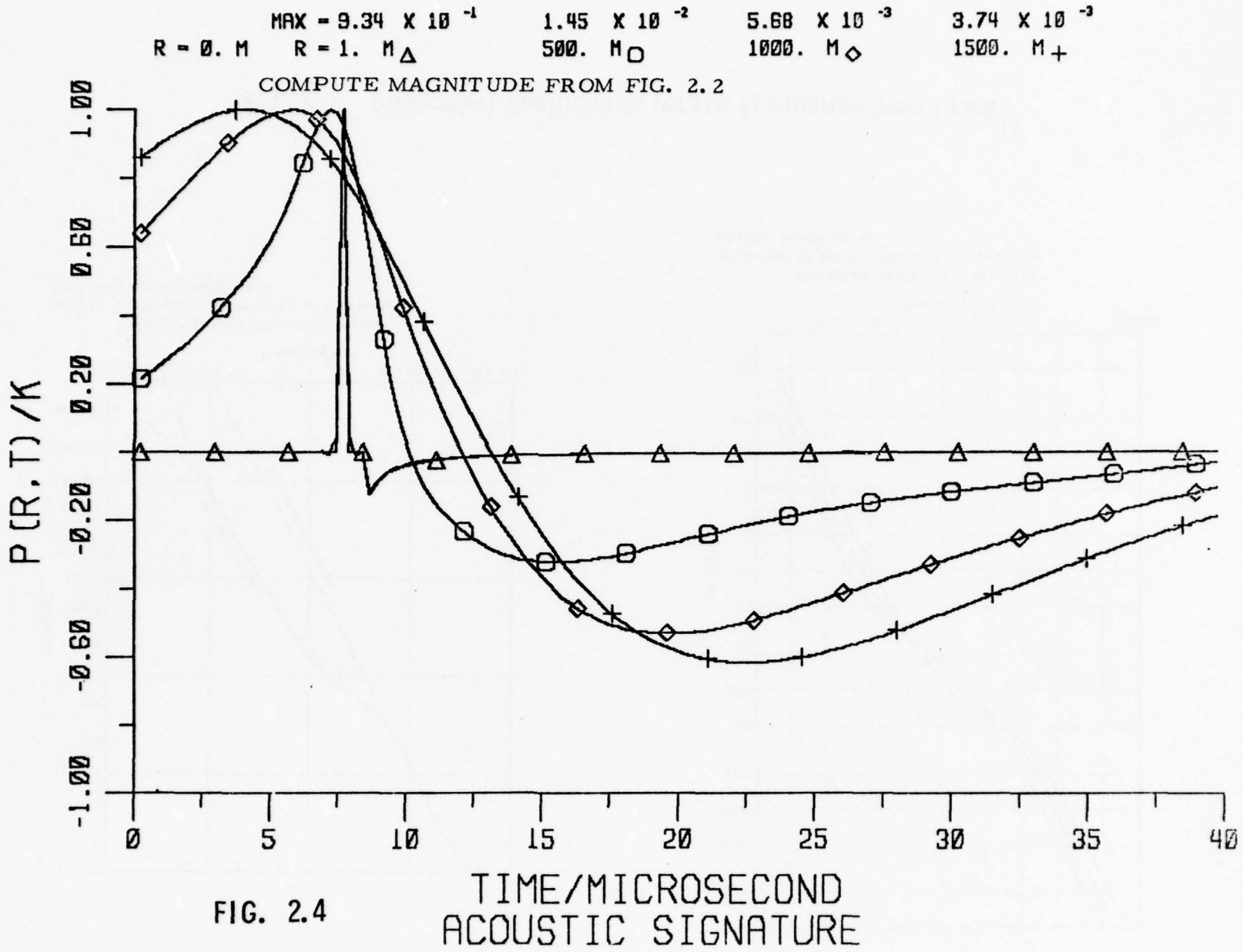

FIG. 2.4 ACOUSTIC SIGNATURE

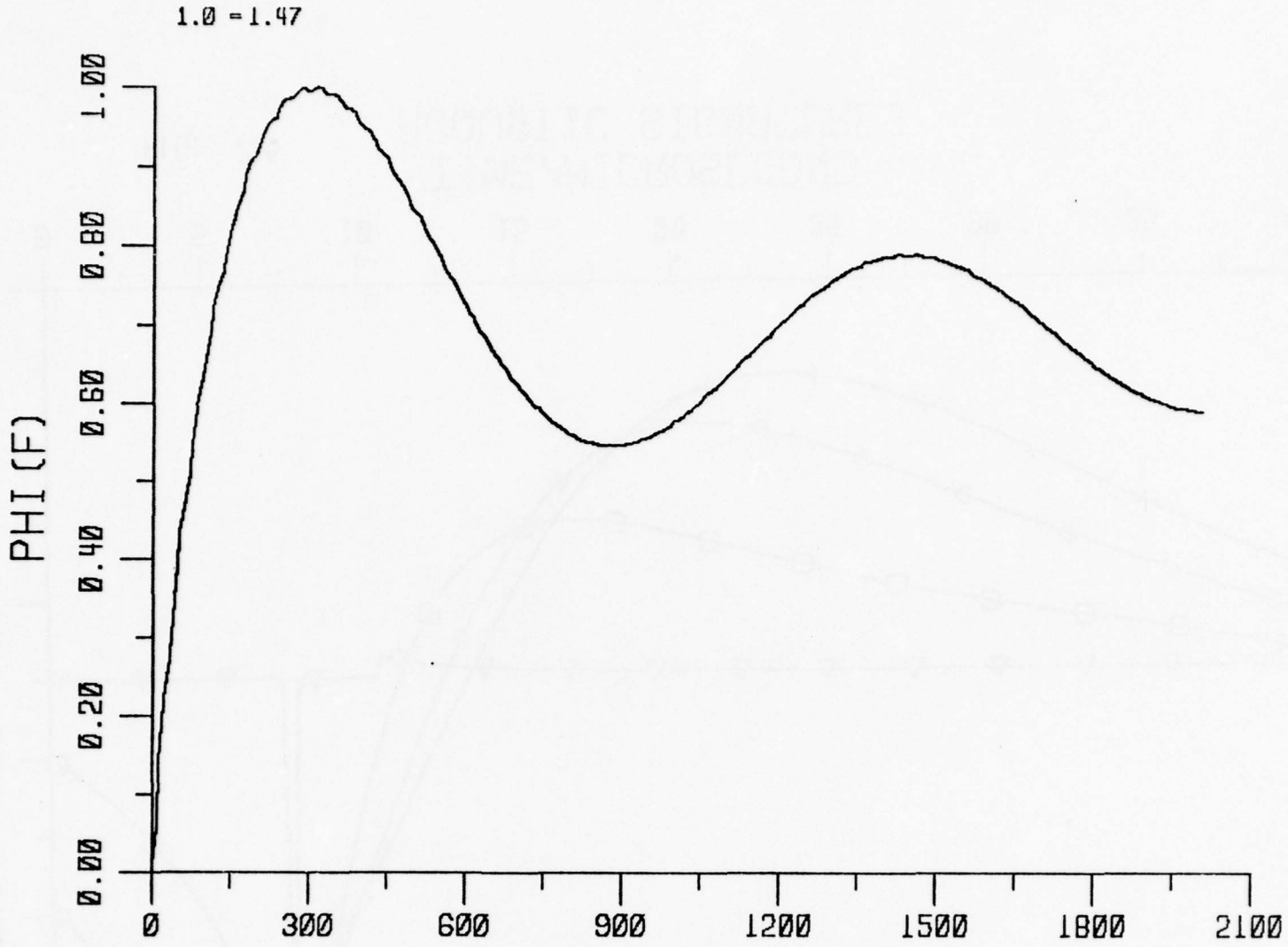
1.0 = 1.47
PHI(F)
0.00
0.20
0.40
0.60
0.80
1.00
0
300
600
900
1200
1500
1800
2100
FREQUENCY/KHZ
ENERGY SPECTRAL DENSITY

FIG. 2.5

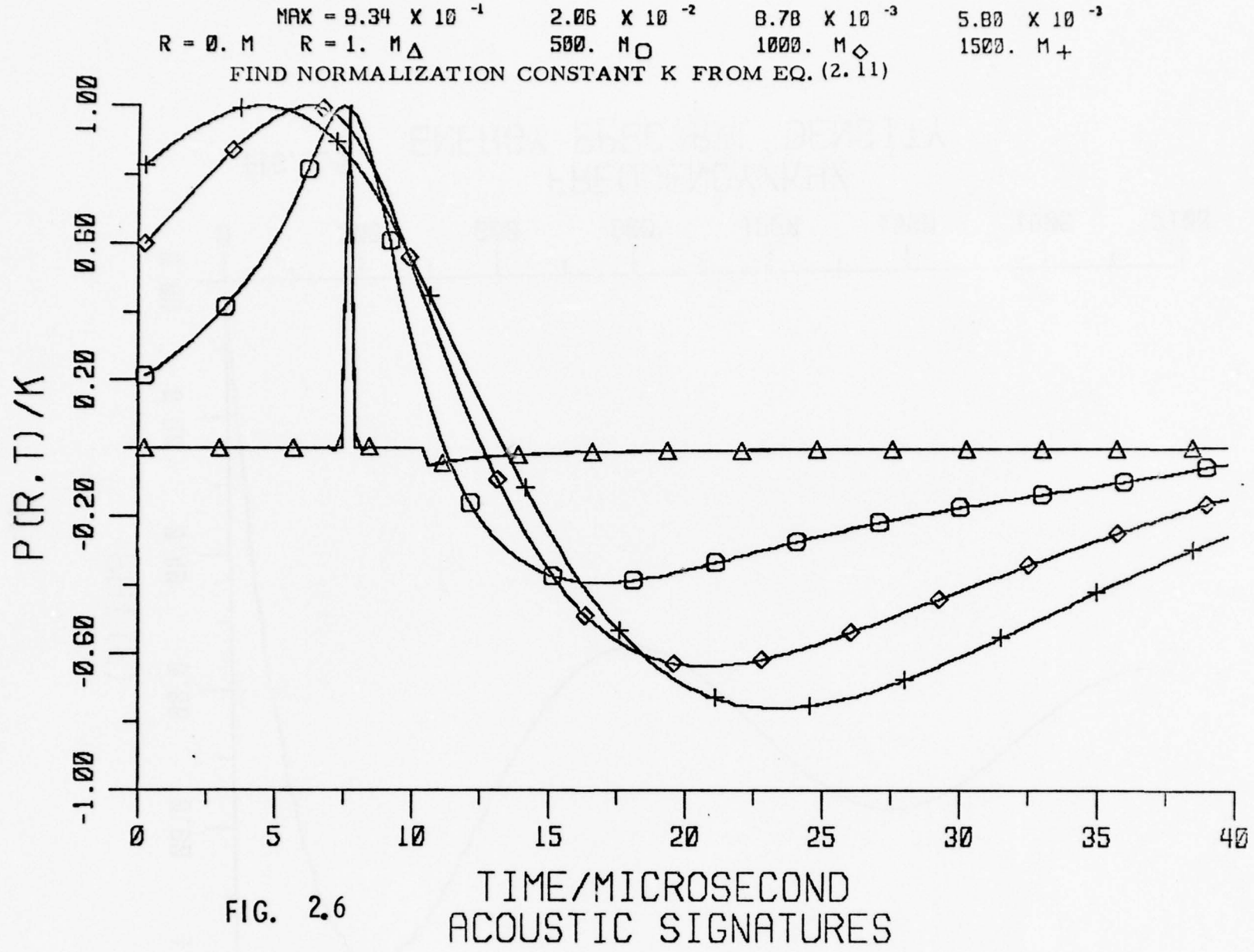
MAX = 9.34 X 10 -1
2.06 X 10 -2
8.78 X 10 -3
5.80 X 10 -3
R = 0. M
R = 1. M Δ
500. M □
1000. M ◇
1500. M +
FIND NORMALIZATION CONSTANT K FROM EQ. (2.11)
P(R,T)/K
1.00
0.60
0.20
-0.20
-0.60
-1.00
0
5
10
15
20
25
30
35
40
TIME/MICROSECOND
ACOUSTIC SIGNATURES

FIG. 2.6

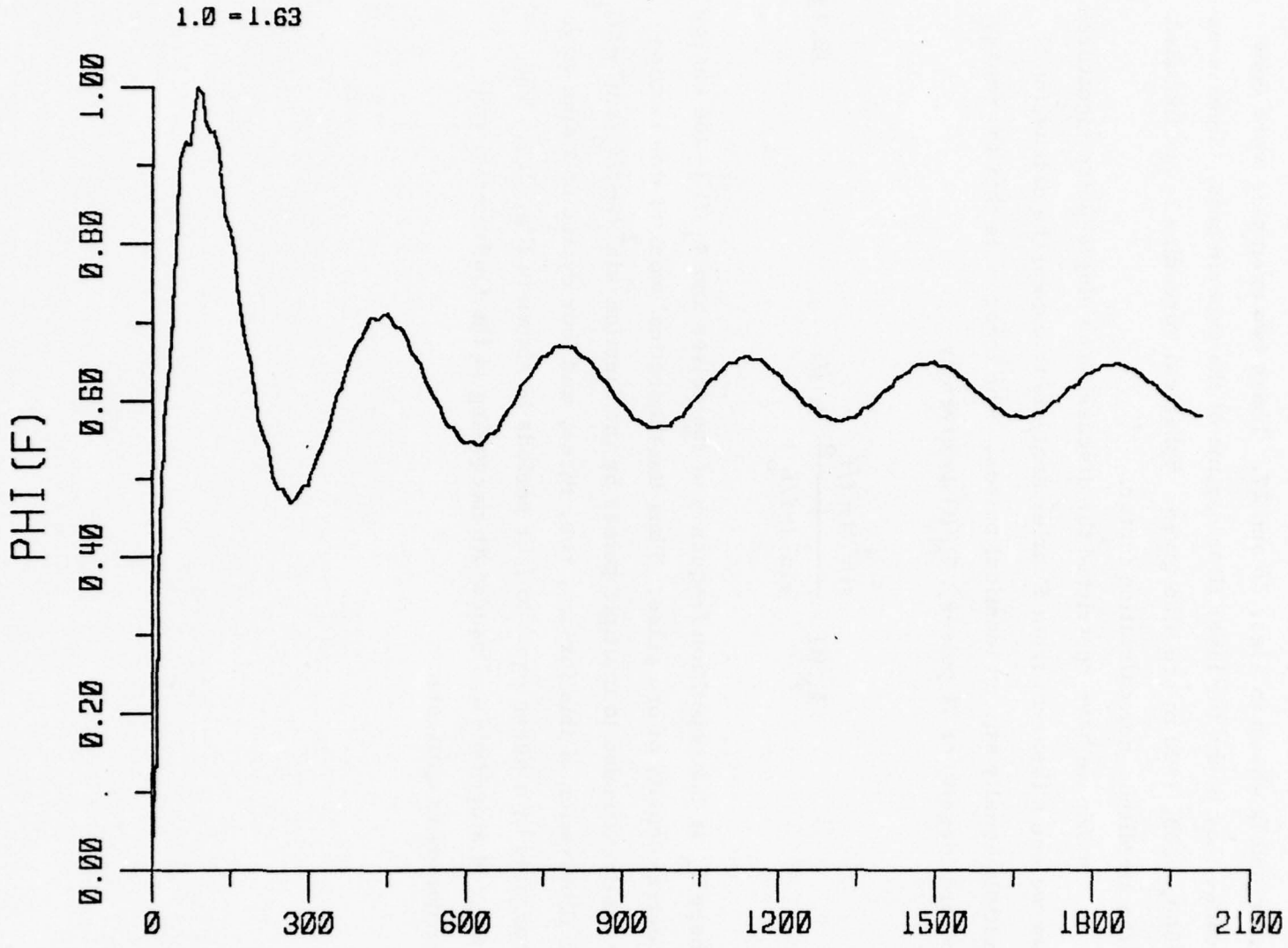
1.0 = 1.63
PHI(F)
0.00
0.20
0.40
0.60
0.80
1.00
0
300
600
900
1200
1500
1800
2100
FREQUENCY/KHZ
ENERGY SPECTRAL DENSITY

FIG. 2.7

3 μsec and is shown in Figs. 26 and 27. These two examples were done because they bound the laser time regime of the experiments. Signatures at 500, 1000, 1500 m are also given. Spherical spreading is not included in the amplitude-normalization factor.

So far we have restricted the discussion to single-pulse signatures. Now we use a theorem from Fourier analysis to extend the discussion to multiple equally spaced identical pulses. The theorem is that the energy spectral density of N pulses, $\Phi_N(f)$ is given by

$$\Phi_N(f) = \frac{\sin^2 N\pi f/f_o}{\sin^2 (\pi f/f_o)} \Phi_1(f) \quad , \tag{2.13}$$

where f_o is the repetition frequency of the pulses and $\Phi_1(f)$ is the energy spectral density of one pulse. Thus the theoretical work of this section is easily extended to multiple pulses by the function $\sin^2 N\pi f/f_o / \sin^2 \pi f/f_o$. An illustration of this for one, two, three, and four cycles of a sine wave separated by a space equal to four periods is shown in Fig. 2.8. The enhanced amplitude and bandwidth narrowing of the fundamental and harmonics is apparent.

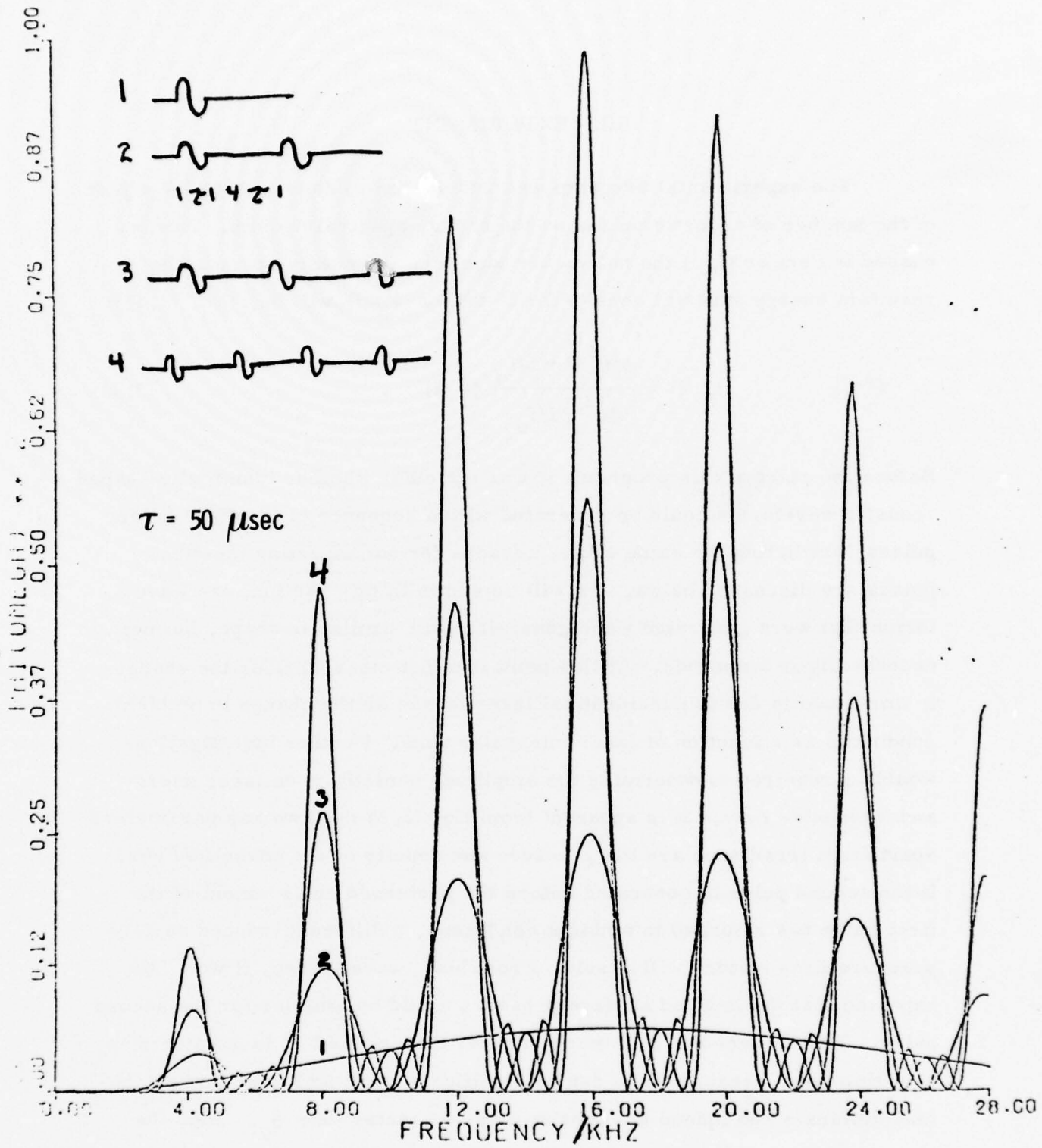
1
2
τ1τ4τ1
3
4
τ = 50 μsec
1.00
0.87
0.75
0.62
0.50
0.37
0.25
0.12
4.00
8.00
12.00
16.00
20.00
24.00
28.00
FREQUENCY /KHZ

Fig. 2.8

III. EXPERIMENT

The experimental program was undertaken to demonstrate the effect of the number of acoustic pulses on the energy spectral density. As discussed in Section II, if the pulses are identical and evenly spaced, the resultant energy spectral density for N pulses $\Phi_N(f)$ will be, (Eq. (2.13);

$$\Phi_N(f) = \frac{\sin^2 N \pi f/f_o}{\sin^2 \pi f/f_o} \Phi_1(f) \quad . \tag{3.1}$$

Before the start of this program, it was not clear whether identically shaped acoustic waveforms could be generated with a sequence of identical laser pulses irradiating the same spot. Reasons for not expecting identical pulses are discussed below. As will be shown in this section, the waveforms that were generated were generally very similar in shape, but not necessarily in amplitude. At this point it is not clear whether the change in amplitude is due to non-identical laser pulses or the change in ambient conditions as a function of laser interpulse time. Further investigations would be required to determine the amplitude sensitivity on laser energy and interpulse time. It is apparent from Eq. (2.5) that two key parameters apart from irradiance are the pressure and density of the unshocked gas. If the second pulse is generated before the perturbed environment of the first pulse has returned to ambient conditions, a different induced surface pressure time history will result. From blast wave theory, it would be expected that the induced surface pressure would be smaller for the second pulse. This is because ρ is much smaller than ρ_o and p is greater than p_o. However, because there can be significant mass addition, this effect may dominate and indeed the density may be greater than ρ_o. Then the

second pulse really is traveling into a denser gas than ambient and the induced surface pressure could well be enhanced. This behavior will be discussed again in this section when two pulses were very closely spaced.

The laser system assembled to investigate multiple pulse radiation induced sound is composed of four K-103 CO_2 laser kits purchased from Lumonics Research Ltd. of Canada. These four TEA lasers are charged from one high-voltage power supply, and triggered individually from a four-channel variable-delay trigger generator. Therefore one, two, three, or four laser pulses were obtained with various interpulse times. A schematic diagram of the experiment appears in Fig. 3-1.

The CO_2 TEA laser is a short-pulse laser. Typically the output pulse of such a laser has a very short high-power spike followed by a lower-power but longer "tail". This "tail" can contain up to 2/3 of the total laser energy. The experiments consisted of operating the lasers with a flowing gas mixture of $He:N_2:CO_2$ of 5:1.6:1.0 SCFH measured with flow meters calibrated for air. The laser capacitors were charged to 35 kV, and had an output of approximately 7 J. This output energy was the result of a tradeoff with pulse-to-pulse stability. The pulse shape was monitored with an L-401 pyroelectric detector manufactured by Barnes Engineering. Figure 3-2 is a representative trace of the detector output. We observe a spike and a tail of several μsec duration. The laser energy was monitored with a 50 D pyroelectric energy meter manufactured by Lumonics. The amplitude of the approximately 50 msec wide pulse is proportional to the laser pulse energy.

The four channel trigger generator was designed and built by Physical Sciences Inc. A "bounceless" switch utilizing a monolithic timing circuit (Signetics NE555 timer) fed four 556 dual timers whose output signals were amplitifed to yield the required trigger voltage amplitude (approximately 15 volts). The laser beams were directed to focusing

Fig. 3.1 Experiment Schematic

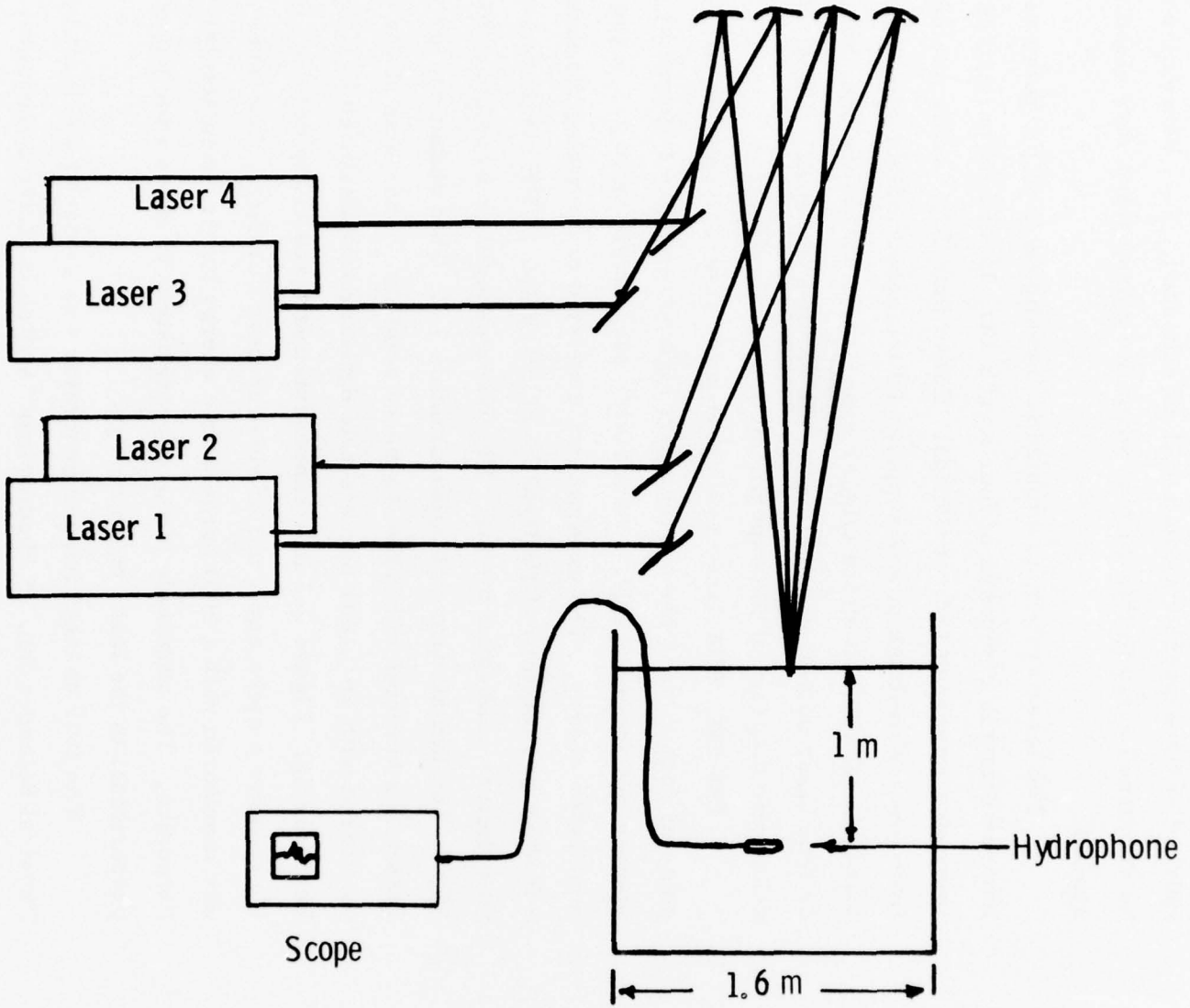

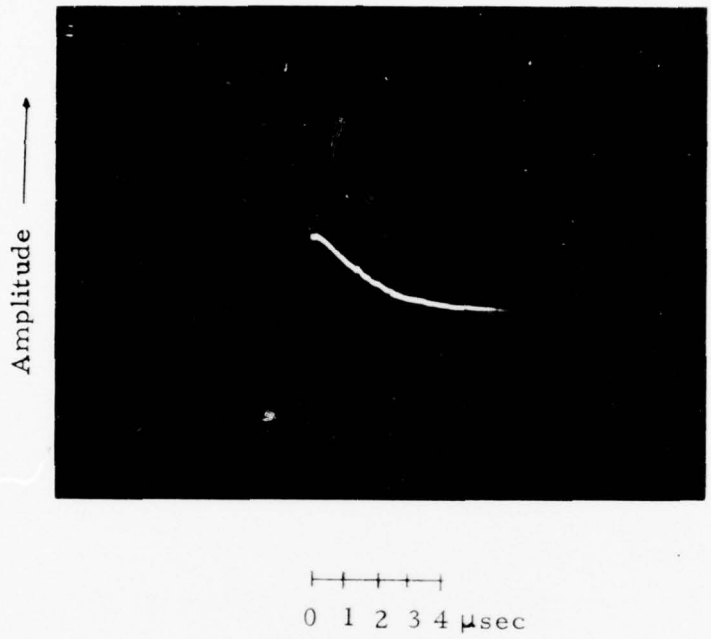

Fig. 3.2 Laser Pulse

mirrors by four gold coated flat mirrors. Four 2.5 m focal length copper mirrors focused the laser beams to approximately the same spot on the water in a large tank. The worst error in location was approximately one-half the beam size. The rectangular laser beam at the water surface was 0.8 x 1.6 cm, measured from a burn pattern. The laser energy with this area corresponds to a fluence of 6 J/cm^2. The tank was 1.6 m in diameter, 1.8 m high and it was filled with water to a depth of 1.4 m.

The acoustic signature was detected with an LC-5-2 hydrophone manufactured by Celesco. The hydrophone has a nominal bandwidth of 500 kHz, although calibration above 100 kHz is not available from the manufacturer. The calibration curve is reproduced in Fig. 3.3. From the calibration information, the average free field sensitivity is -126.9 dB re 1 volt/μbar which corresponds to 0.452 $V/10^6$ $dynes/cm^2$. The calibration at 100 kHz will be used (-128 dB) because 100 kHz is representative of the frequency peak of the spectrum. The sensitivity is 0.40 $V/10^6$ $dynes/cm^2$.

A series of one, two, three, and four laser pulse experiments was performed. A number of representative experimental traces will be discussed in detail. Many other experimental traces were obtained, but will not be discussed in this report. The data were captured by photographing a Tektronix 475 oscilloscope trace. The resultant photograph was digitized from a magnified copy of the original photograph. A minimal distortion of approximately 1% is introduced in this process. The waveforms that were analyzed are tabulated in Table II along with the number of pulses and the interpulse time. The amplitudes will be evident in the computer-generated plots of these waveforms.

The waveforms and spectra of these waveforms will now be discussed. A single pulse waveform is shown in Fig. 3.4, where the vertical

LC 5-2 TRANSDUCER SERIAL NO. 408
AVERAGE FREE FIELD VOLTAGE SENSITIVITY -126.9db

FREQUENCY IN KHz
METHOD OF CALIBRATION: COMPARISON
WITH STANDARD LC-32 SERIAL NO. 1200
WATER TEMPERATURE 22 °C. DEPTH 10 FT.
TEST TECHNICIAN
QUALITY CONTROL

CABLE LENGTH 5 FT
CAPACITANCE W/CABLE 340 Pf
DC RESISTANCE 50K MEGOHMS
MOUNTING SLEEVE LEAKAGE
RESISTANCE ——— MEGOHMS
DATE 8-26-76 BY CLS

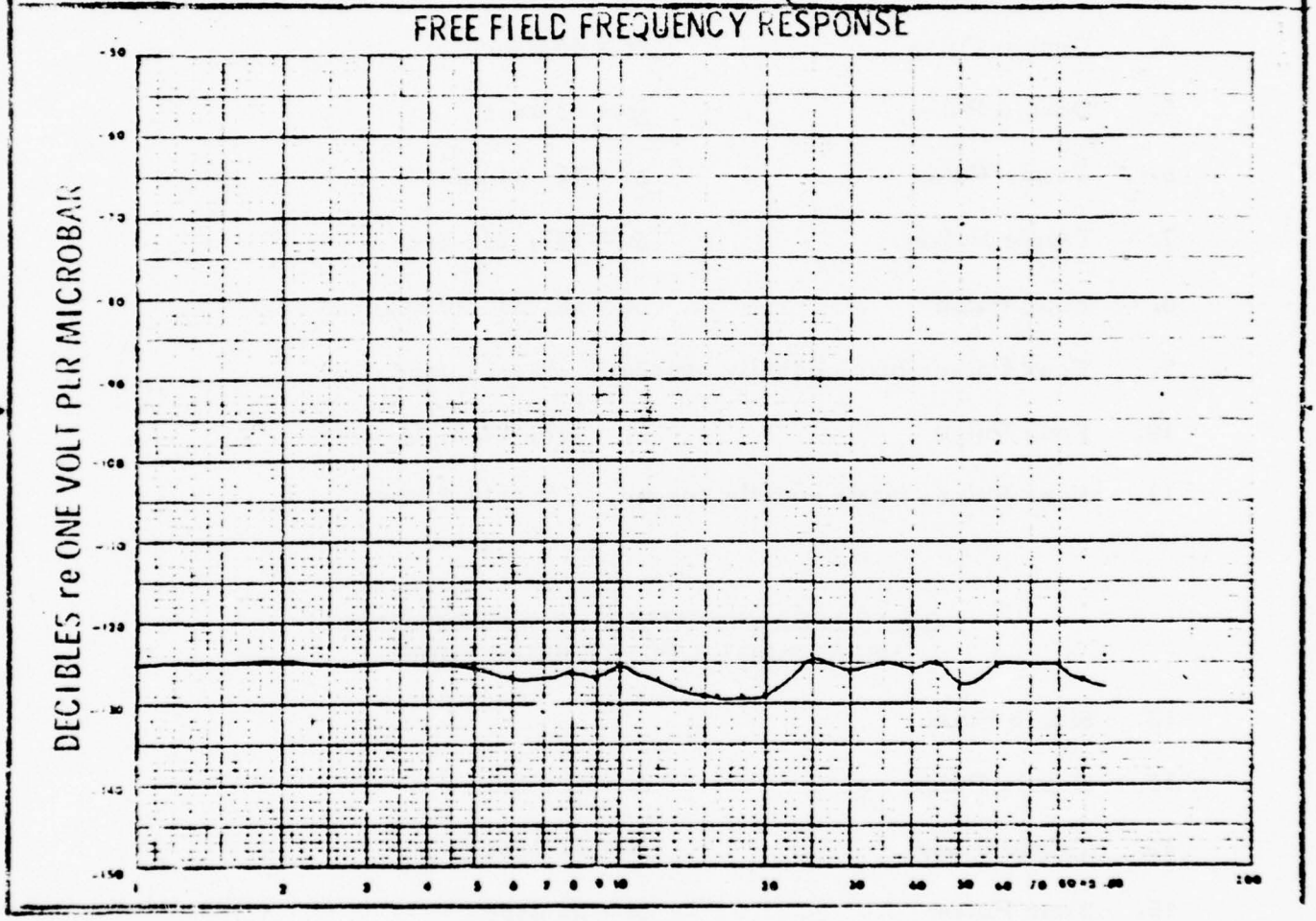

Fig. 3.3 Hydrophone Calibration

TABLE II

ANALYZED WAVEFORMS

Laser Fluence Per Pulse = 6 J/cm^2

Threshold Fluence ~ 3J/cm^2

1.	Single Pulse	
2.	Double Pulse	Δt = 15 μsec
3.	Double Pulse	Δt = 20 μsec
4.	Double Pulse	Δt = 45 μsec
5.	Double Pulse	Δt = 3 μsec
6.	Triple Pulse	Δt = 45, 64 μsec
7.	Triple Pulse	Δt = 157, 152 μsec
8.	Four Pulse	Δt = 38, 33, 30 μsec
9.	Four Pulses made equally spaced,	Δt = 31 μsec
10.	Four Pulse	Δt = 115, 17.5, 50 μsec
11.	Four Pulses made equally spaced,	Δt = 17.5 μsec

COMPUTER SYNTHESIZED WAVEFORMS
USING SINGLE PULSE SIGNATURE

12.	Single Pulse	
13.	Double Pulse	Δt = 31 μsec
14.	Triple Pulse	Δt = 31 μsec
15.	Four Pulse	Δt = 31 μsec

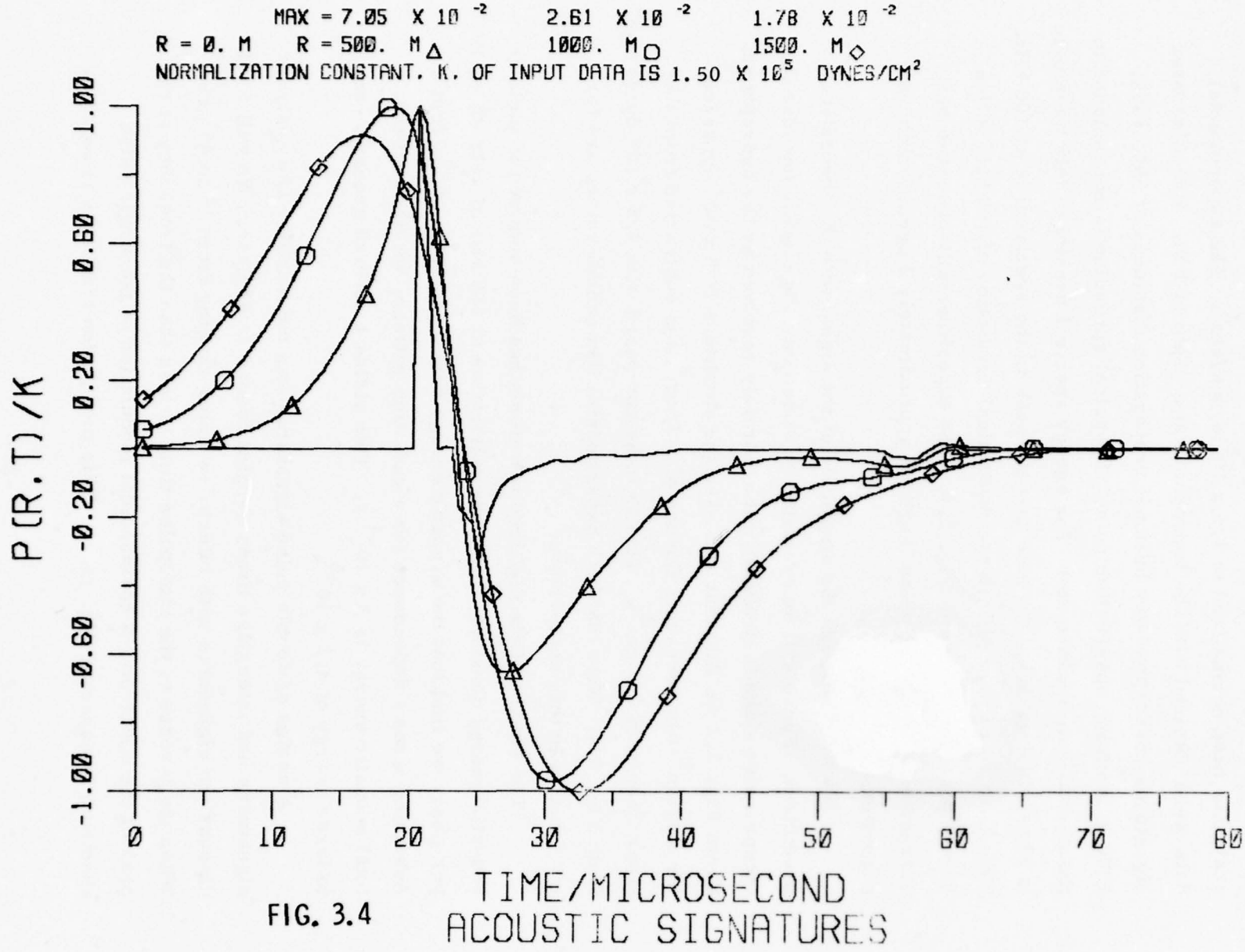

FIG. 3.4 ACOUSTIC SIGNATURES

scale has been normalized to 1.5×10^5 dynes/cm^2. The experimental data were obtained with the hydrophone at a depth of 1 m. The attenuated signatures correspond to additional propagation distances of 500, 1000, 1500 m from the observation point. Spherical spreading is not included in the normalization constants. The energy spectral density of this waveform is shown in Fig. 3.5. We note that the peak in the spectrum is at 100 kHz. This is to be compared with the theoretical prediction of 100 kHz with a 3 μsec pulse, as shown in Fig. 2.6. The experimentally observed peak corresponds to a laser pulse length of approximately 3 μsec, which was observed, see Fig. 3.2.

We now compare the amplitude of the signal with the theoretical prediction. These will be evaluated at 5 μsec into the signal, because the compressive spike is probably not accurately resolved by the hydrophone. From Fig. 2.2 we find that at 5 μsec the amplitude is 8×10^4 dynes/cm^2 for 3 J/cm^2 (the threshold fluence of 3 J/cm^2 was subtracted from the laser fluence of 6 J/cm^2). This is to be compared with 4.5×10^4 dynes/cm^2 from Fig. 3.4. Note that both experimental theoretical values are for r = 1 meter in this comparison.

The square of the digitized waveform has been summed to yield an acoustic energy density. Using the calibration at 100 kHz of -128 dB re 1V per μbar, we find that the acoustic energy density is 1.5×10^{-8} J/cm^2. Assuming a $\cos\theta$ dependence for a radiation pattern, we find that the total acoustic energy is 3×10^{-4} J. This yields a ratio of acoustic energy to laser energy of 4.2×10^{-5}.

A series of double pulse signatures was measured. The analyzed signatures had interpulse times ranging from 3 to 45 μsec. We will first discuss the signatures with interpulse times ranging from 15 to 45 μsec. When the inverse of the interpulse time is less than the frequency at the peak of the spectrum, a cosinusoidal modulation of the single pulse spectrum is expected (Eq. (3.1)). This modulation frequency is equal to

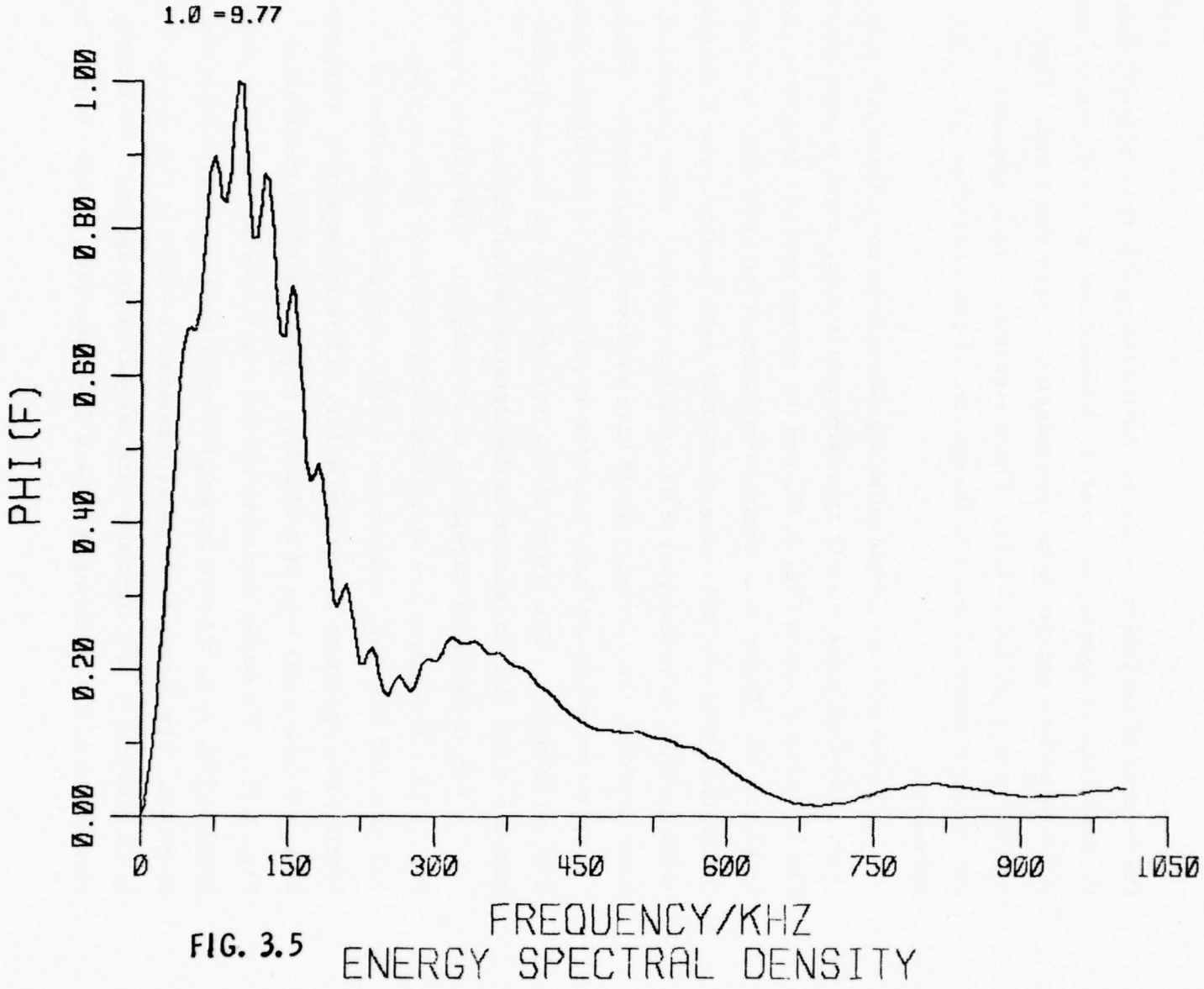
1.0 =9.77
PHI(F)
0.00
0.20
0.40
0.60
0.80
1.00
0
150
300
450
600
750
900
1050
FREQUENCY/KHZ
ENERGY SPECTRAL DENSITY

FIG. 3.5

the inverse of the interpulse time. As the interpulse time is lengthened, the modulation frequency is lowered. Three double pulse signatures and their respective spectra have been selected to show this trend. These are shown in Figs. 3.6 to 3.11. These signatures are in sequence of increasing number of peaks in the spectra as the modulation frequency decreases.

The remaining double pulse signature to be considered is a special case. The interpulse time is approximately 3 μsec, which is very small. The signal is shown in Fig. 3.12, and the energy spectral density is given in Fig. 3.13. There is no cosine modulation of the spectrum, and while not an ideal example, this case shows that wehn the interpulse time gets short enough, no modulation of the spectrum occurs. If the pulses had been identical, the spectrum would have narrowed significantly. Ideally, the spectrum would continue to narrow in proportion to the inverse of the number of pulses. The utility of this type of waveform may be limited because of the high attenuation of the signature with distance.

Two three-pulse waveforms were analyzed. The first is shown in Fig. 3.14. The pulses are almost but not quite evenly spaced, i.e., 157 μsec and 152 μsec, and because of this, the ideal modulation of a single-pulse spectrum illustrated in Fig. 2.8 is not expected. Nevertheless, we do see this type of modulation in portions of the spectrum in Fig. 3.15. We do not expect to see the 1 to 9 ratio of "bump" to peak found in Fig. 2.8, because the amplitudes of the three pulses were not identical. The second three-pulse signature is shown in Fig. 3.16. This is an illustration of a signature with unequal pulse spacing. No simple modulation of the spectrum is expected or observed as shown in Fig. 3.17.

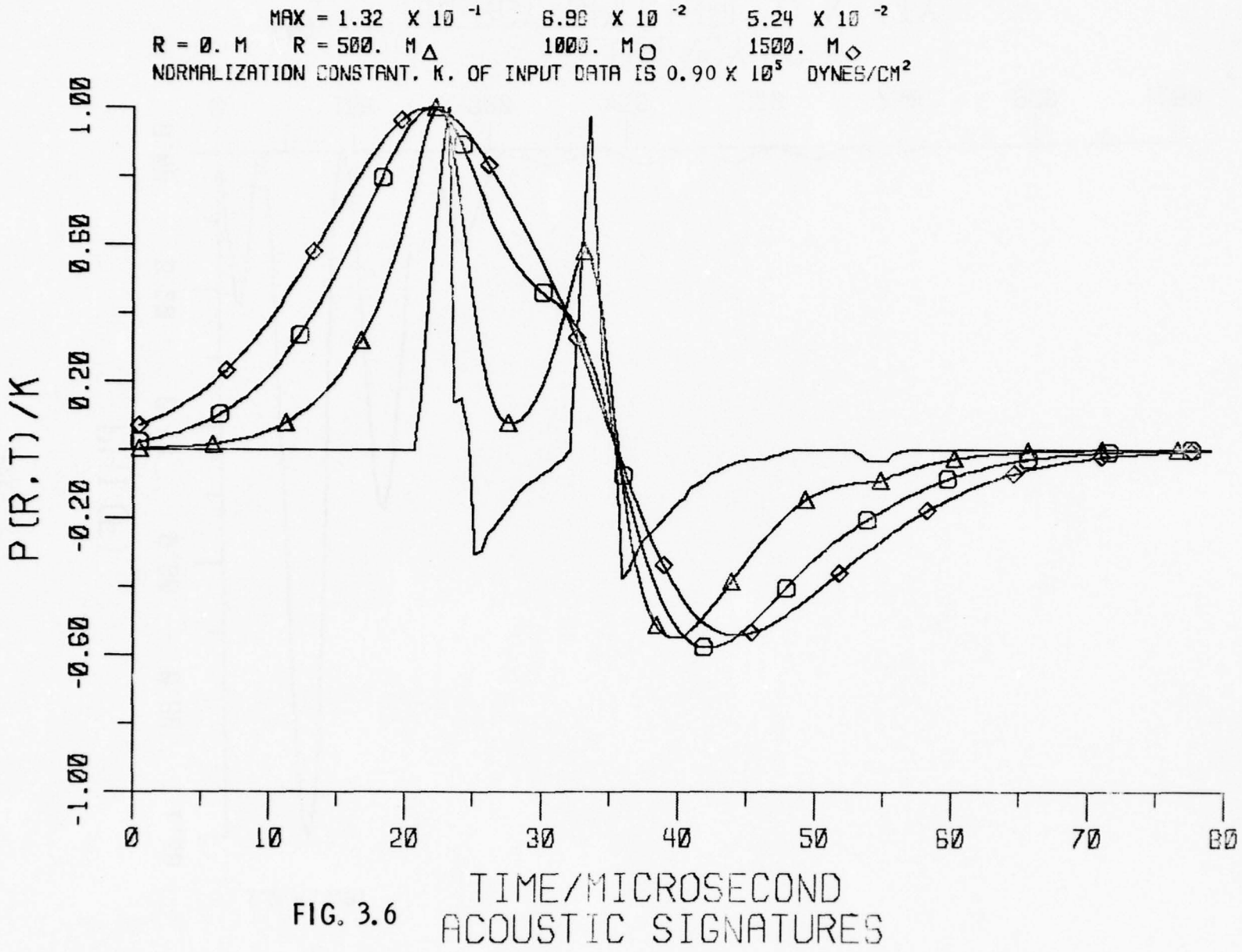

FIG. 3.6 ACOUSTIC SIGNATURES

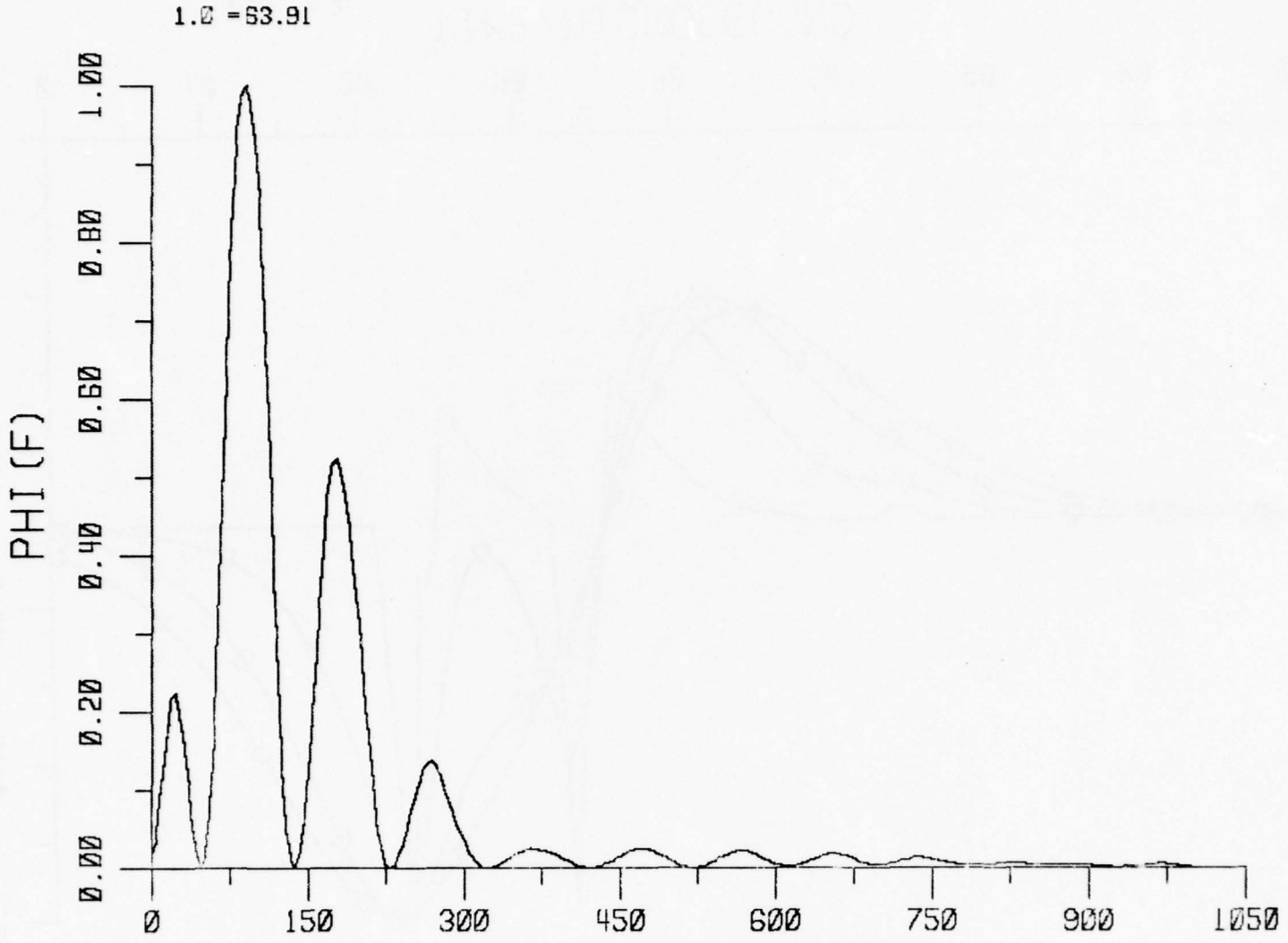
1.0 =53.91
PHI(F)
0.00
0.20
0.40
0.60
0.80
1.00
0
150
300
450
600
750
900
1050
FREQUENCY/KHZ
ENERGY SPECTRAL DENSITY

FIG. 3.7

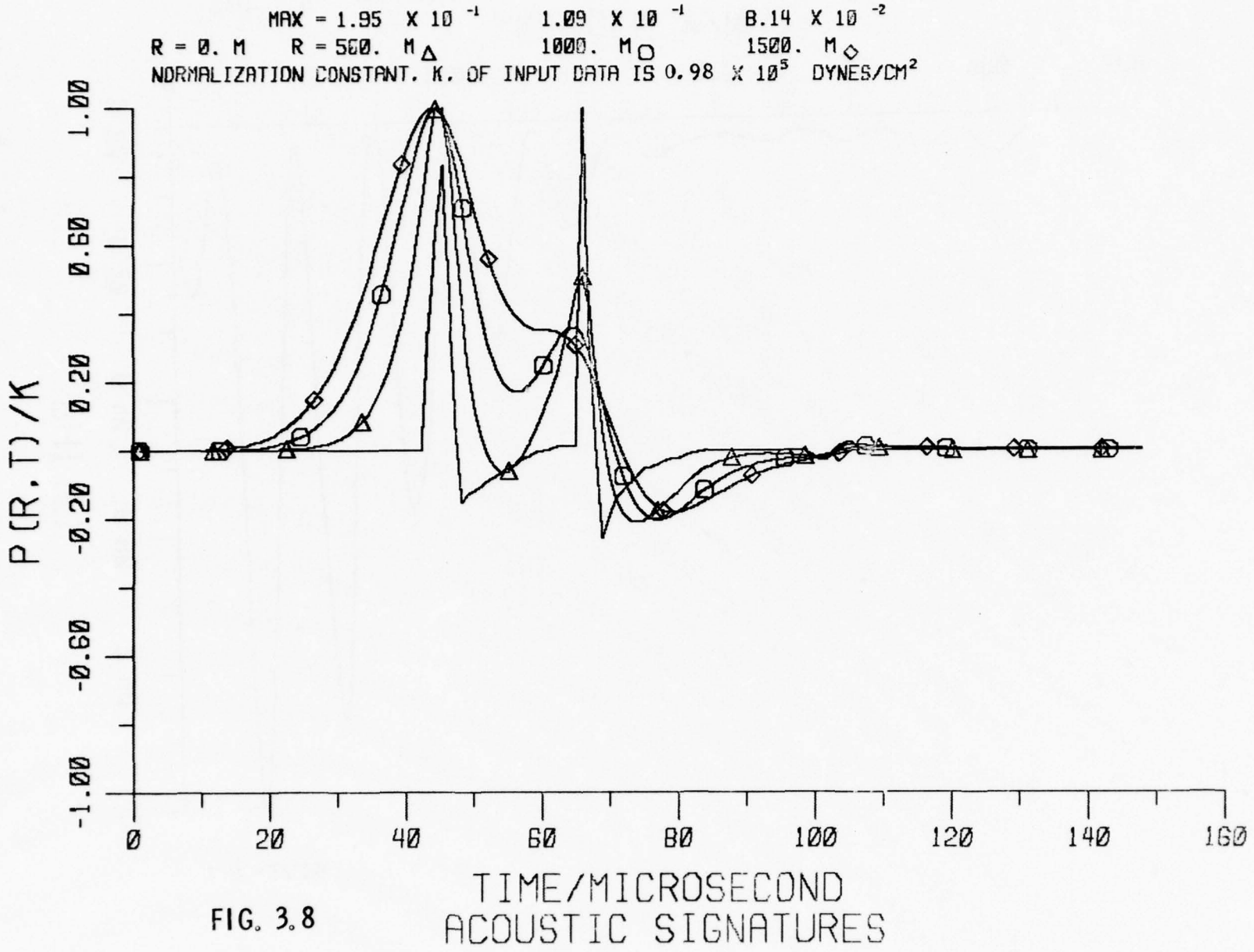

FIG. 3.8 ACOUSTIC SIGNATURES

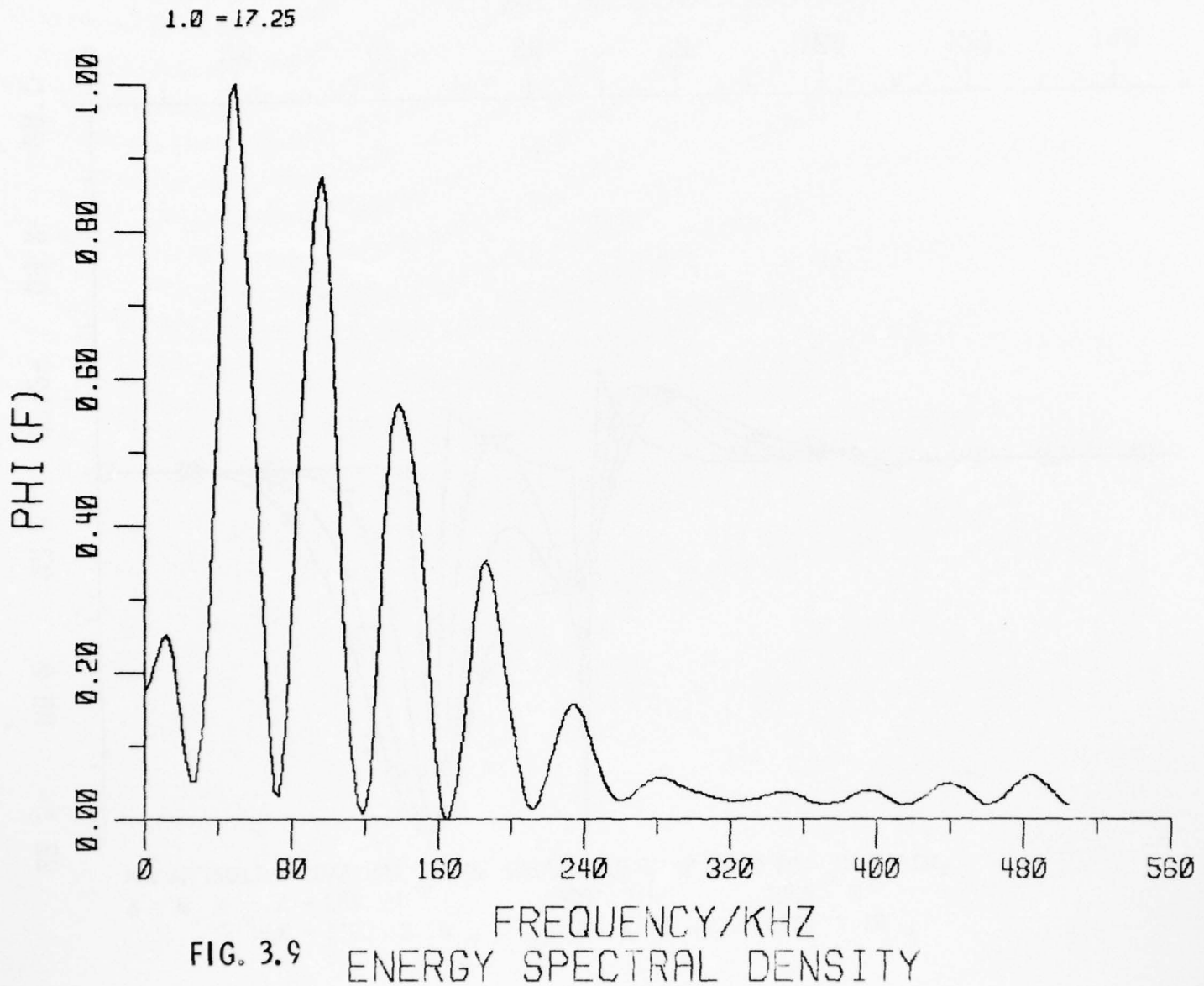
1.0 = 17.25
PHI(F)
0.00
0.20
0.40
0.60
0.80
1.00
0
80
160
240
320
400
480
560
FREQUENCY/KHZ
ENERGY SPECTRAL DENSITY

FIG. 3.9

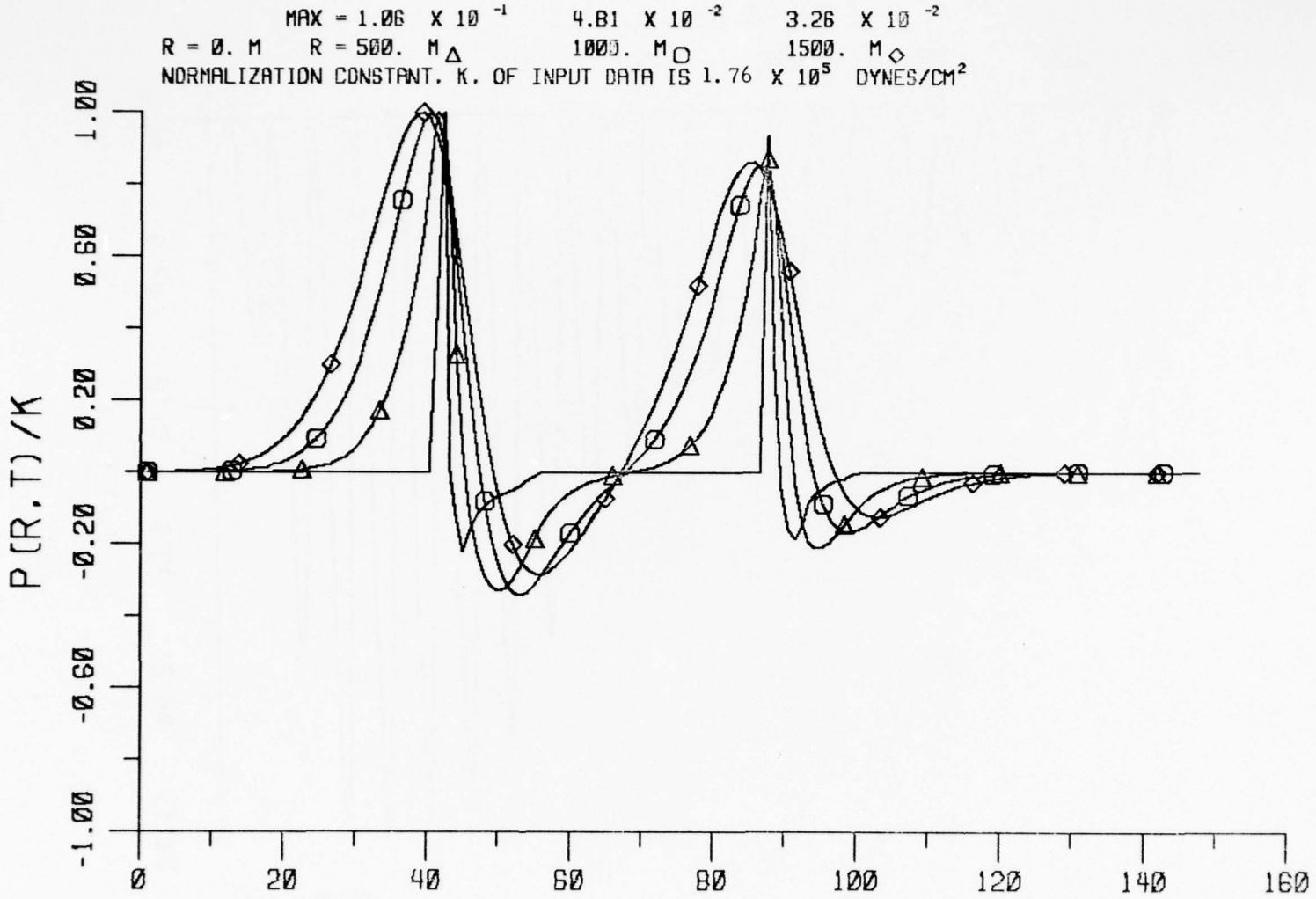

FIG. 3.10 ACOUSTIC SIGNATURES

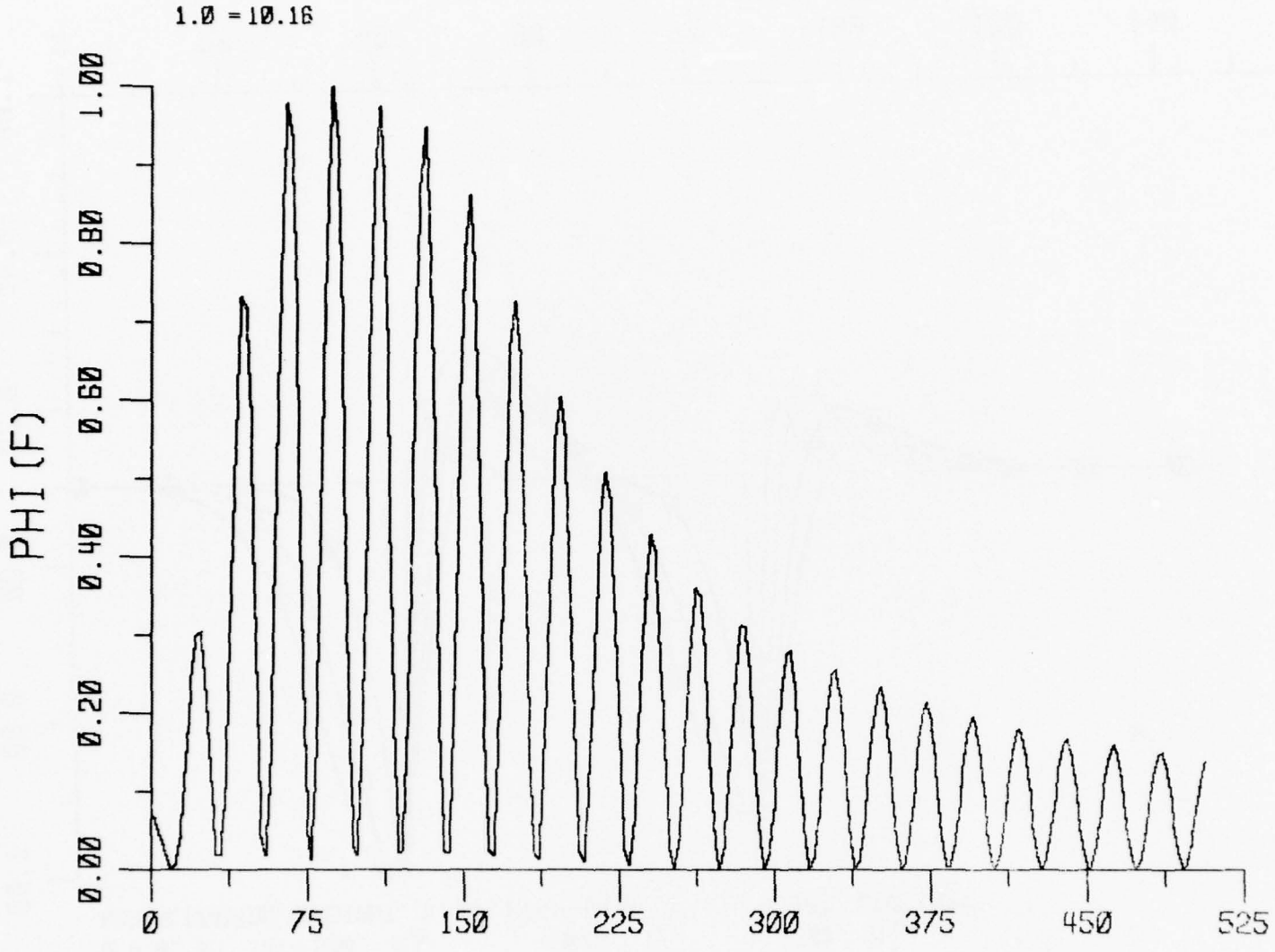

FIG. 3.11 ENERGY SPECTRAL DENSITY

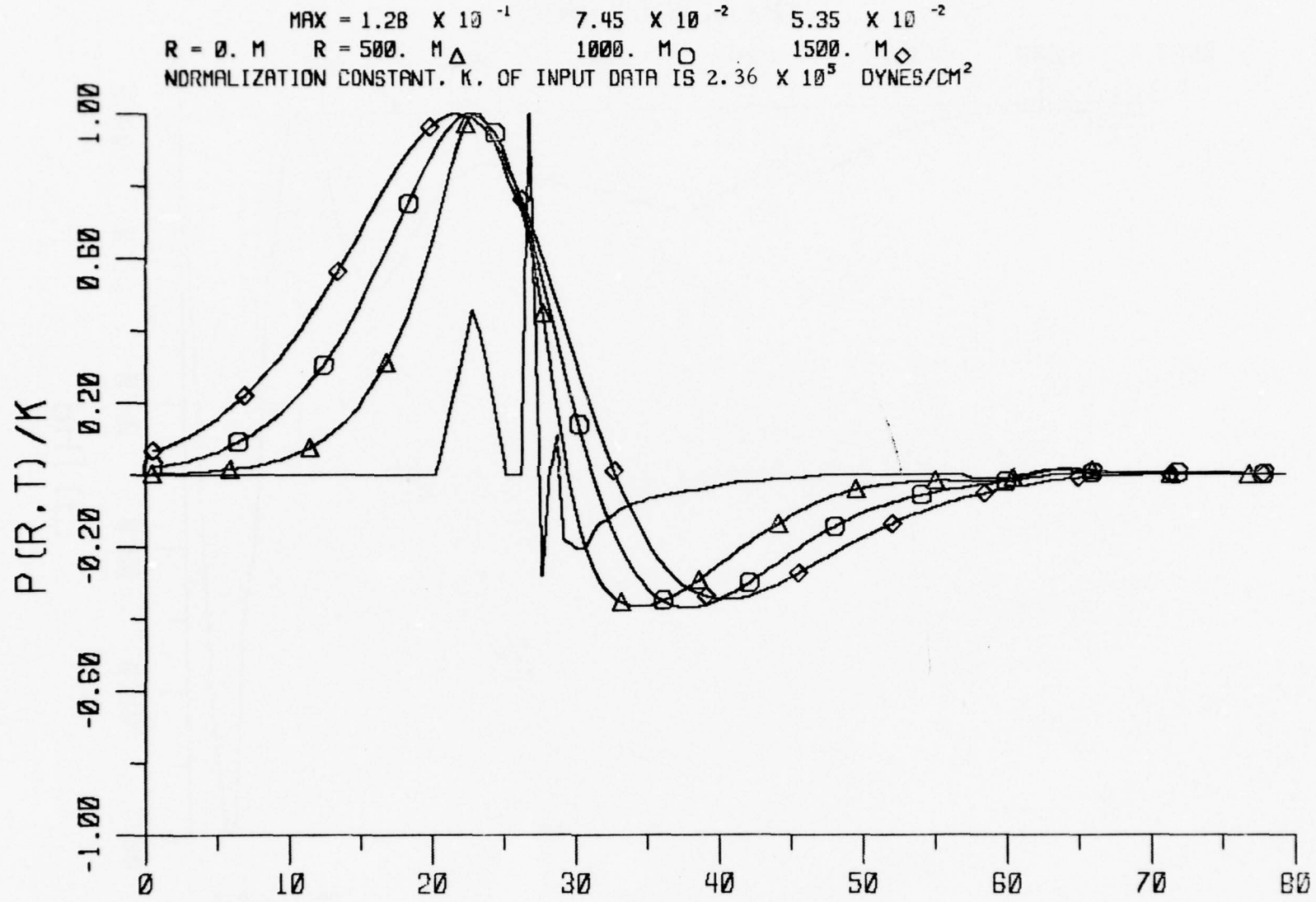

FIG. 3.12 ACOUSTIC SIGNATURES

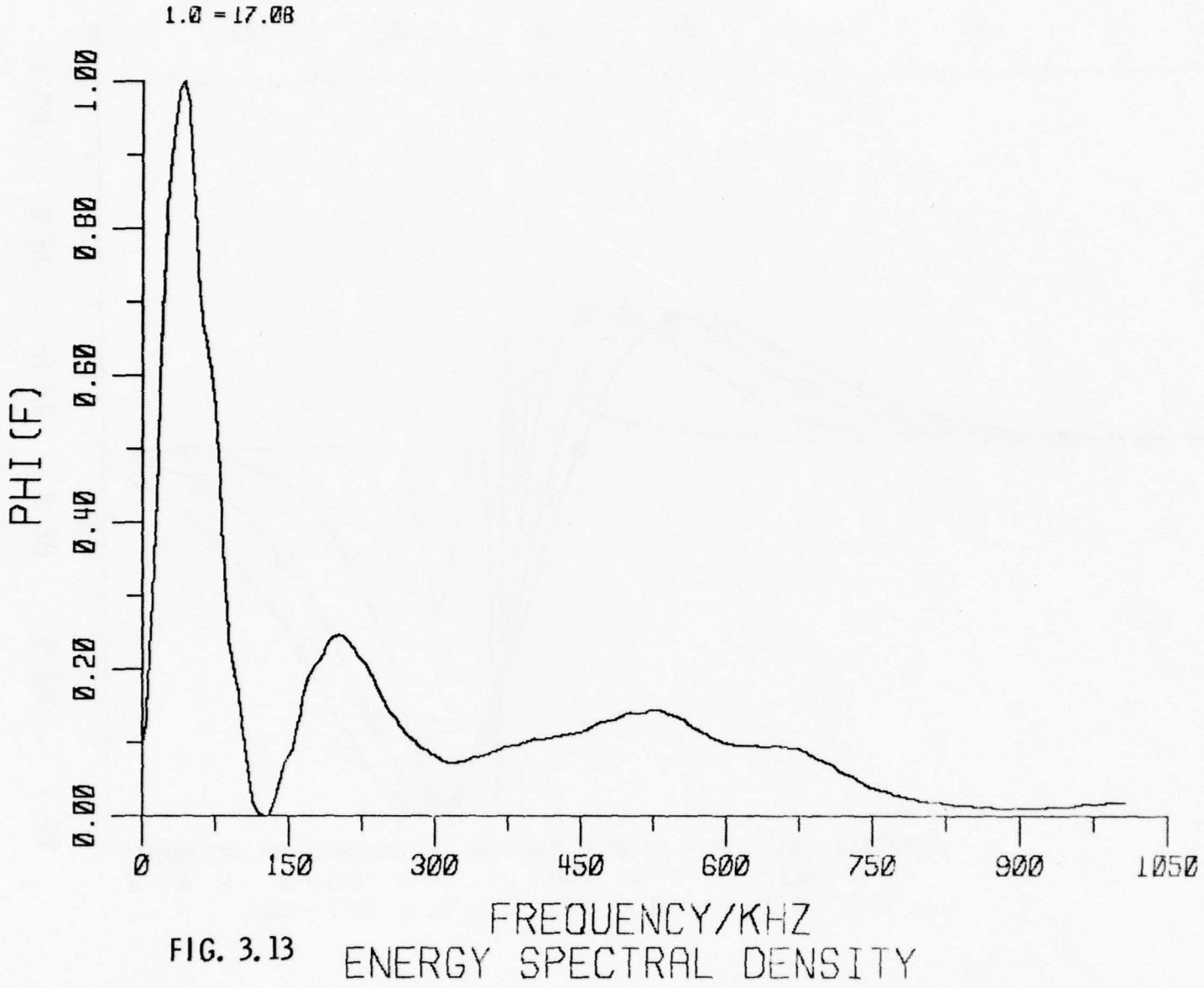
1.0 = 17.08
PHI(F)
0.00
0.20
0.40
0.60
0.80
1.00
0
150
300
450
600
750
900
1050
FREQUENCY/KHZ
ENERGY SPECTRAL DENSITY

FIG. 3.13

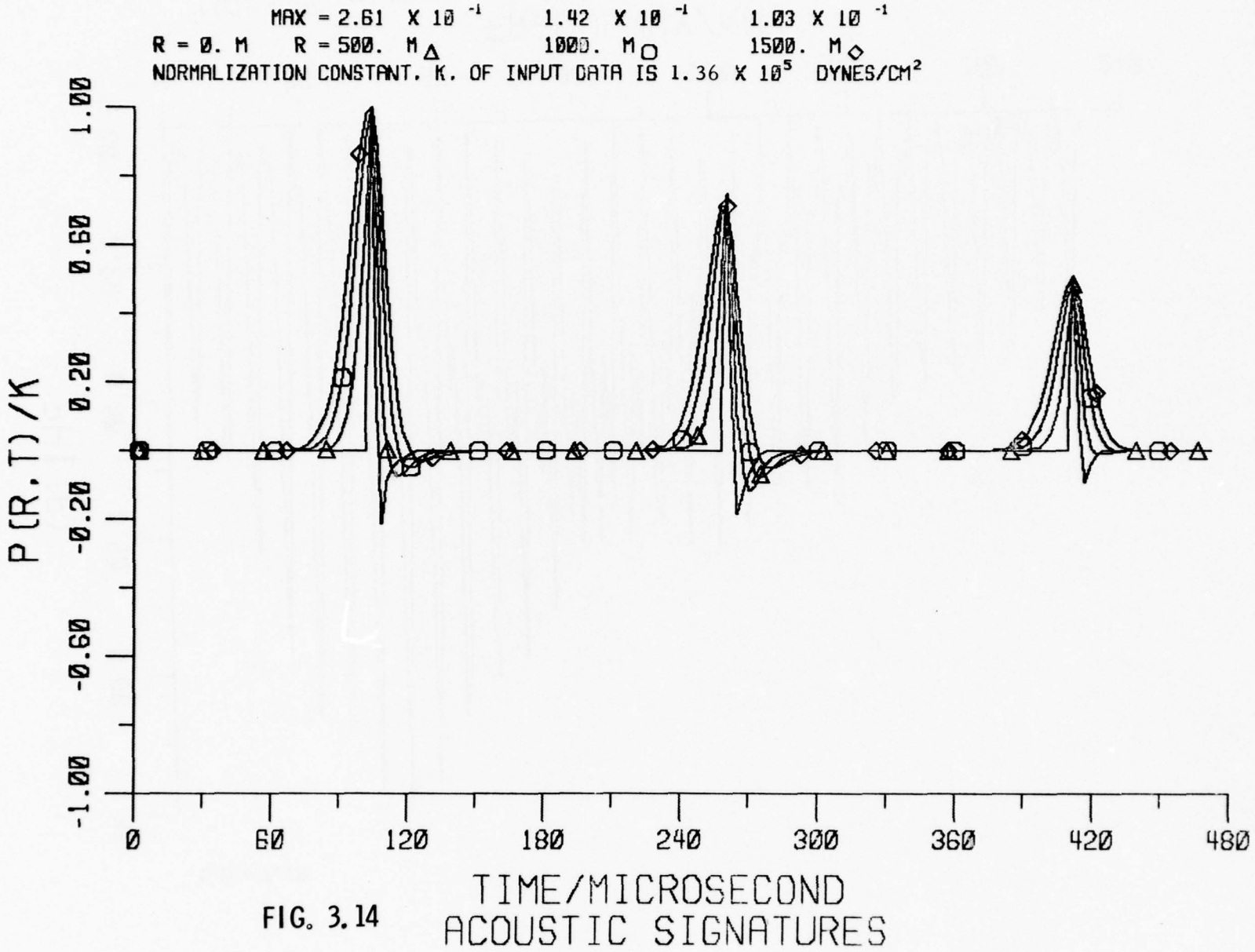
MAX = 2.61 X 10 -1
1.42 X 10 -1
1.03 X 10 -1
R = 0. M
R = 500. M Δ
1000. M ○
1500. M ◇
NORMALIZATION CONSTANT, K, OF INPUT DATA IS 1.36 X 10^5 DYNES/CM^2
P(R,T)/K
1.00
0.60
0.20
-0.20
-0.60
-1.00
0
60
120
180
240
300
360
420
480
TIME/MICROSECOND
ACOUSTIC SIGNATURES

FIG. 3.14

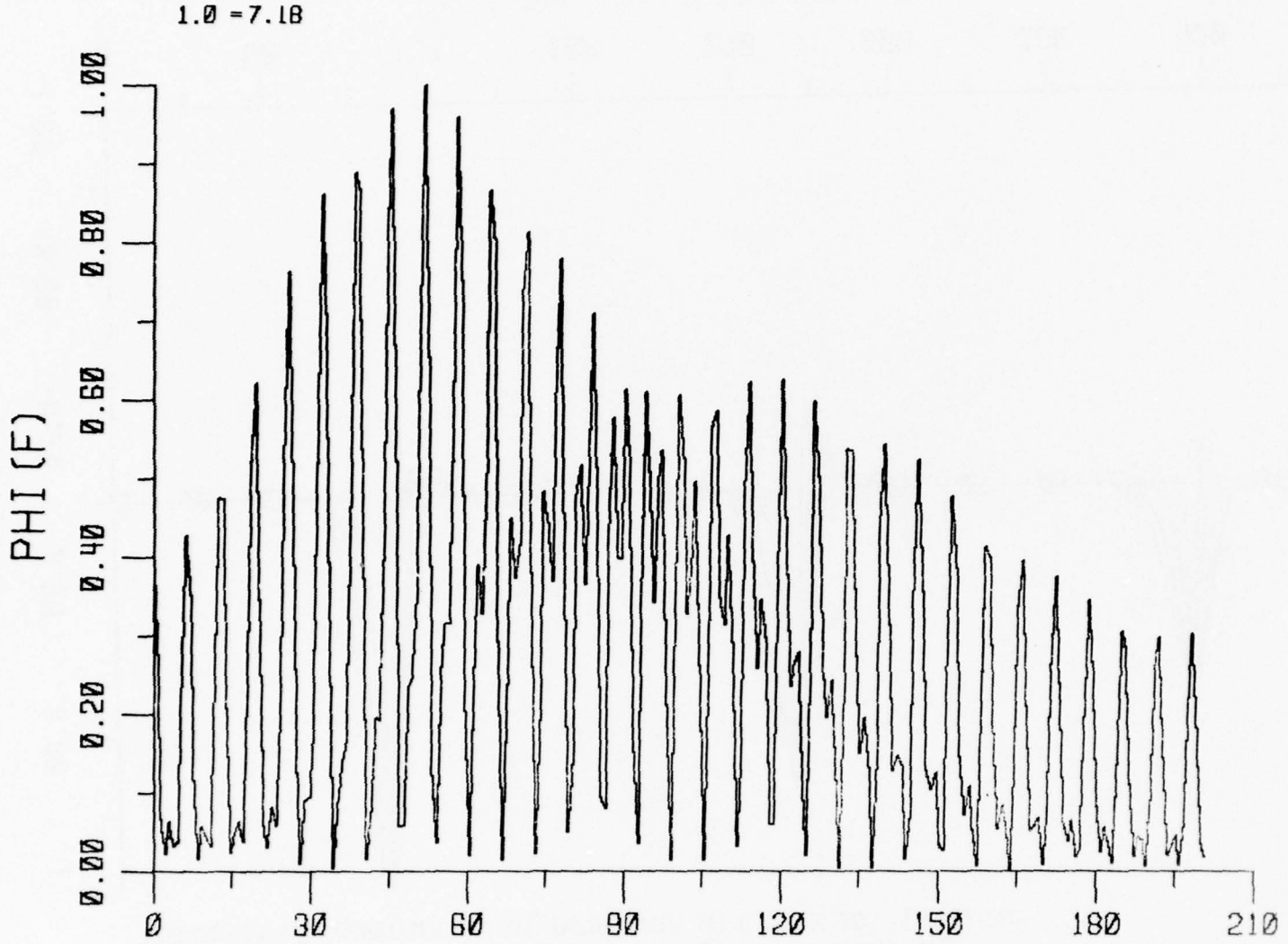
1.0 =7.18
PHI(F)
0.00
0.20
0.40
0.60
0.80
1.00
0
30
60
90
120
150
180
210
FREQUENCY/KHZ
ENERGY SPECTRAL DENSITY

FIG. 3.15

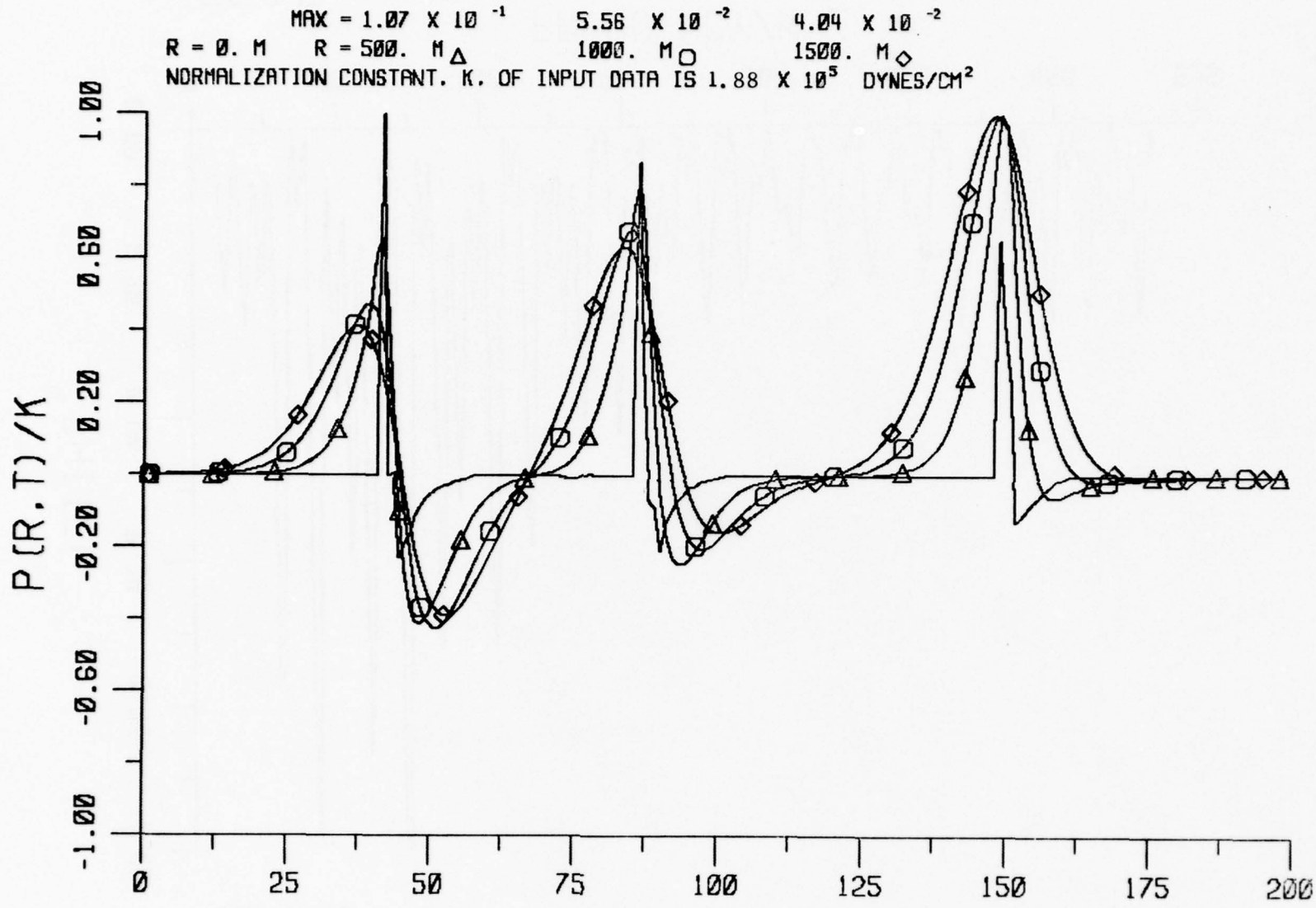

FIG. 3.16 ACOUSTIC SIGNATURES

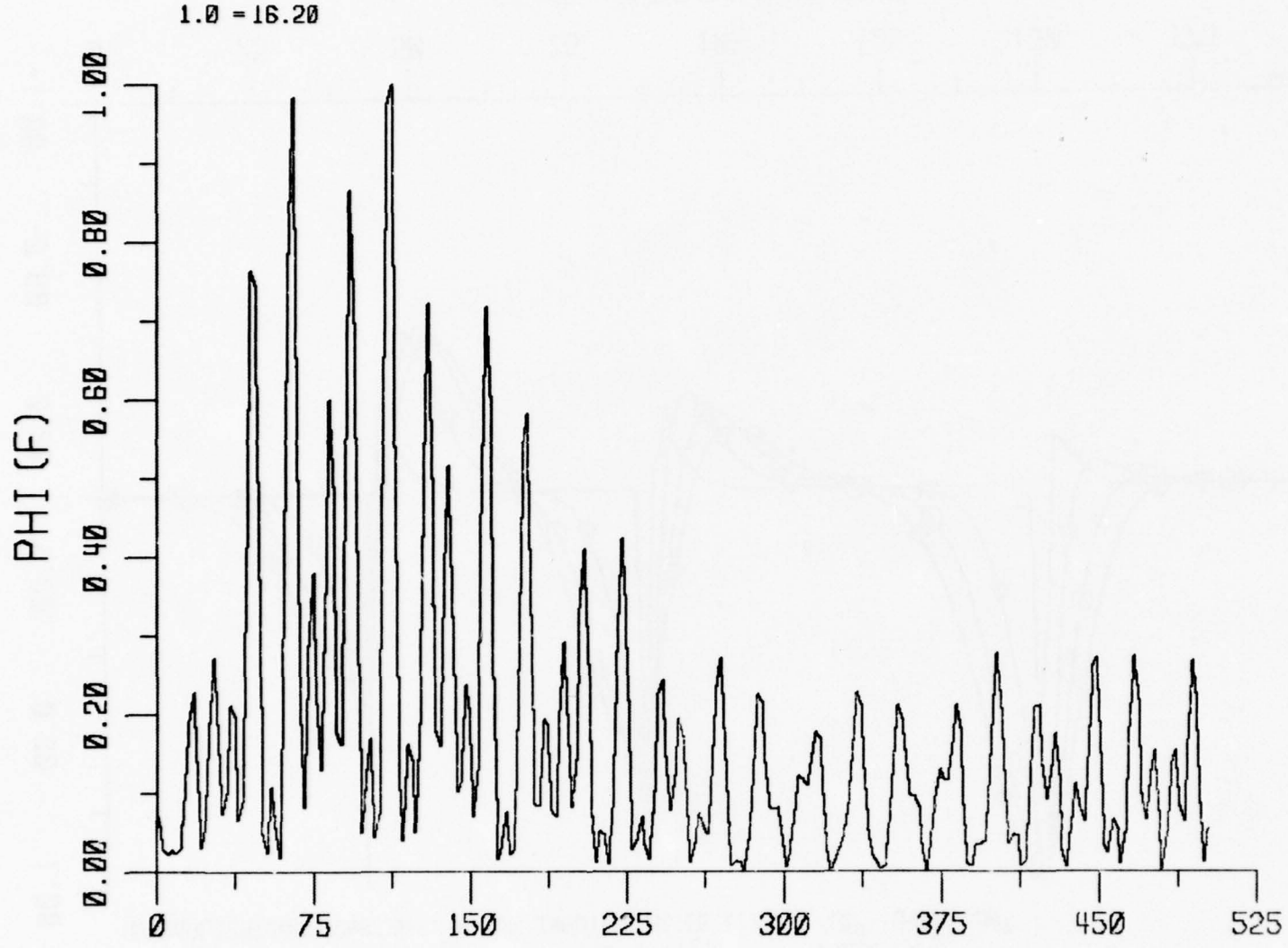
1.0 = 16.20
PHI(F)
0.00
0.20
0.40
0.60
0.80
1.00
0
75
150
225
300
375
450
525
FREQUENCY/KHZ
ENERGY SPECTRAL DENSITY

FIG. 3.17

The first four pulse signature to be analyzed is shown in Fig. 3.18. Unfortunately, the pulses were equal neither in amplitude nor in spacing. The spectrum is given in Fig. 3.19. We note the modulation, but also the lack of any coherent modulation of the spectrum. The pulses were artificially made equally spaced in a computer synthesized signature. This is shown in Fig. 3.20. The spacing was made equal to 31 μsec. We note the more or less coherent modulation of the spectrum in Fig. 3.21. A modulation such as shown in Fig. 2.8 is not expected, because the amplitude of the pulses are not equal - causing the bumps in between the spikes in the spectrum to be larger than for an ideal case.

The second of the four pulse signature is shown in Fig. 3.22. The spacing of the pulses is not uniform, so a ragged spectrum is expected. The spectrum is shown in Fig. 3.23. Indeed the spectrum does not show any repetitive structure. The broad band character is maintained by the unevenly spaced pulses. If the pulses had been evenly spaced, the spectrum would be much more characteristic of Fig. 2.8 for four cycles of a sine wave. An evenly spaced signature was synthesized from Fig. 3.22. This was done by making the pulse separation equal to 17.5 μsec, which is the spacing between the second and third pulse. The signature is shown in Fig. 3.24, and the spectrum is shown in Fig. 3.25. We note the rather significant narrowing of the main spectral components, and also the two double bumps between the peaks in the spectrum. These bumps are very characteristic of a four pulse spectrum; e.g., see Fig. 2.8. The lack of data for evenly spaced pulses is not due to any fundamental physical limitation. When these data were taken, the lasers did not trigger with a stable interpulse time.

In an effort to illustrate the behavior of the signature and spectrum with pulse number, the following computations were made. The single pulse signature of Fig. 3.4 was used as a single pulse signature, and repeated to form a two -, three -, and four - pulse signature (the little bump in the signature at 40 μsec was eliminated). The computed results are given in

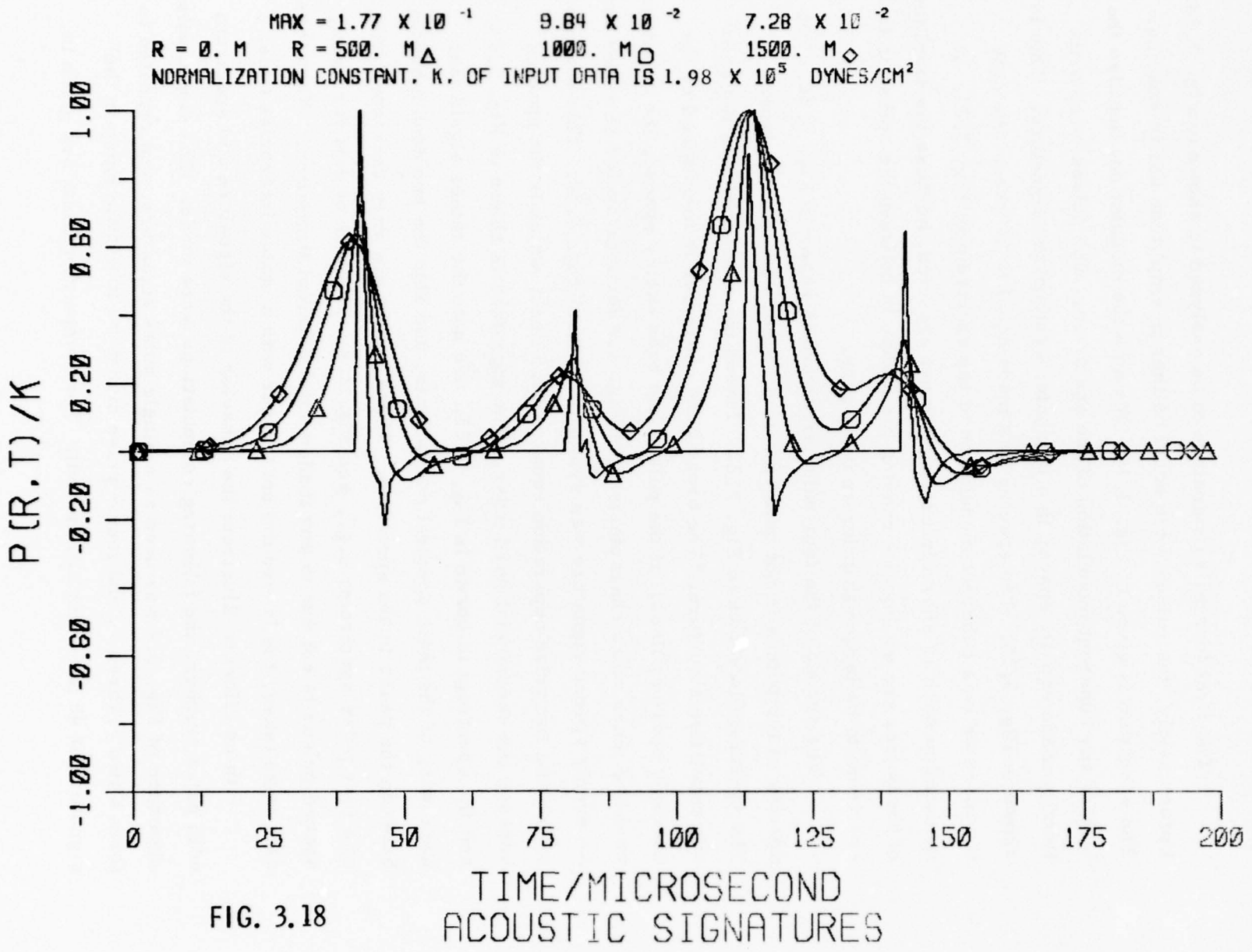

FIG. 3.18 ACOUSTIC SIGNATURES

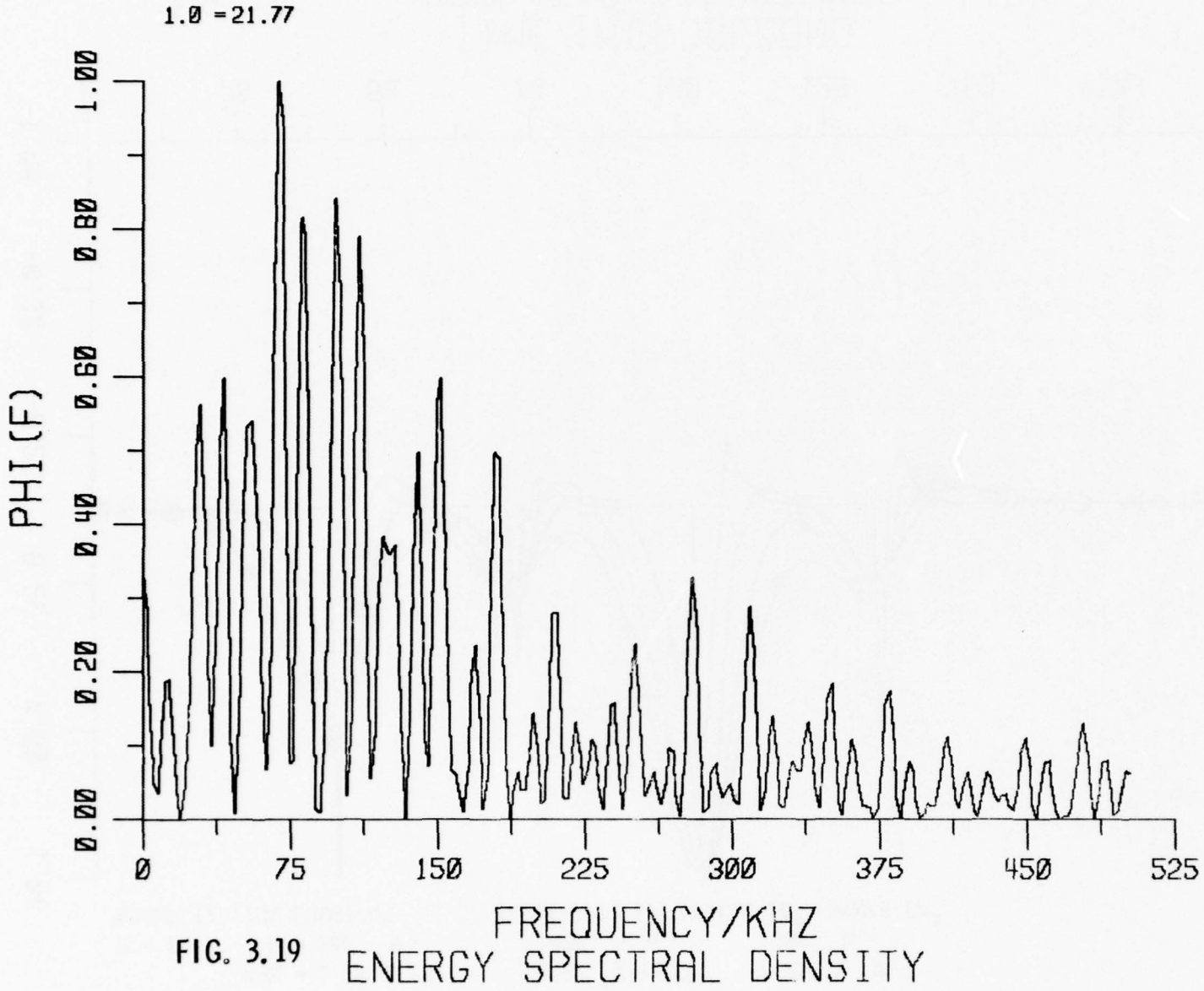
1.0 =21.77
PHI(F)
0.00
0.20
0.40
0.60
0.80
1.00
0
75
150
225
300
375
450
525
FREQUENCY/KHZ
ENERGY SPECTRAL DENSITY

FIG. 3.19

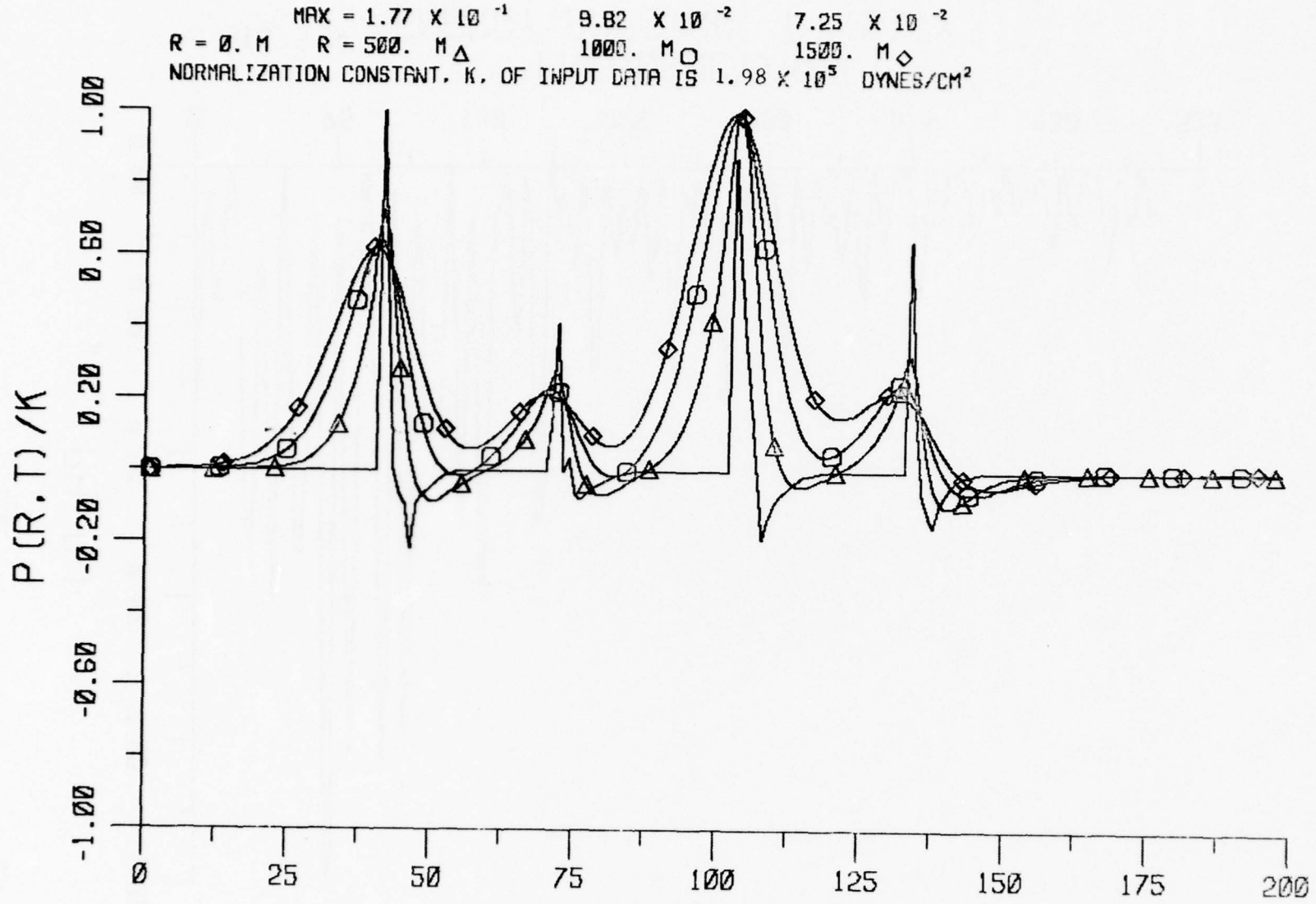
MAX = 1.77 X 10 -1
9.82 X 10 -2
7.25 X 10 -2
R = 0. M
R = 500. M Δ
1000. M O
1500. M ◇
NORMALIZATION CONSTANT, K, OF INPUT DATA IS 1.98 X 10 5 DYNES/CM 2
P(R,T)/K
1.00
0.60
0.20
-0.20
-0.60
-1.00
0
25
50
75
100
125
150
175
200
TIME/MICROSECOND
ACOUSTIC SIGNATURES

FIG. 3.20

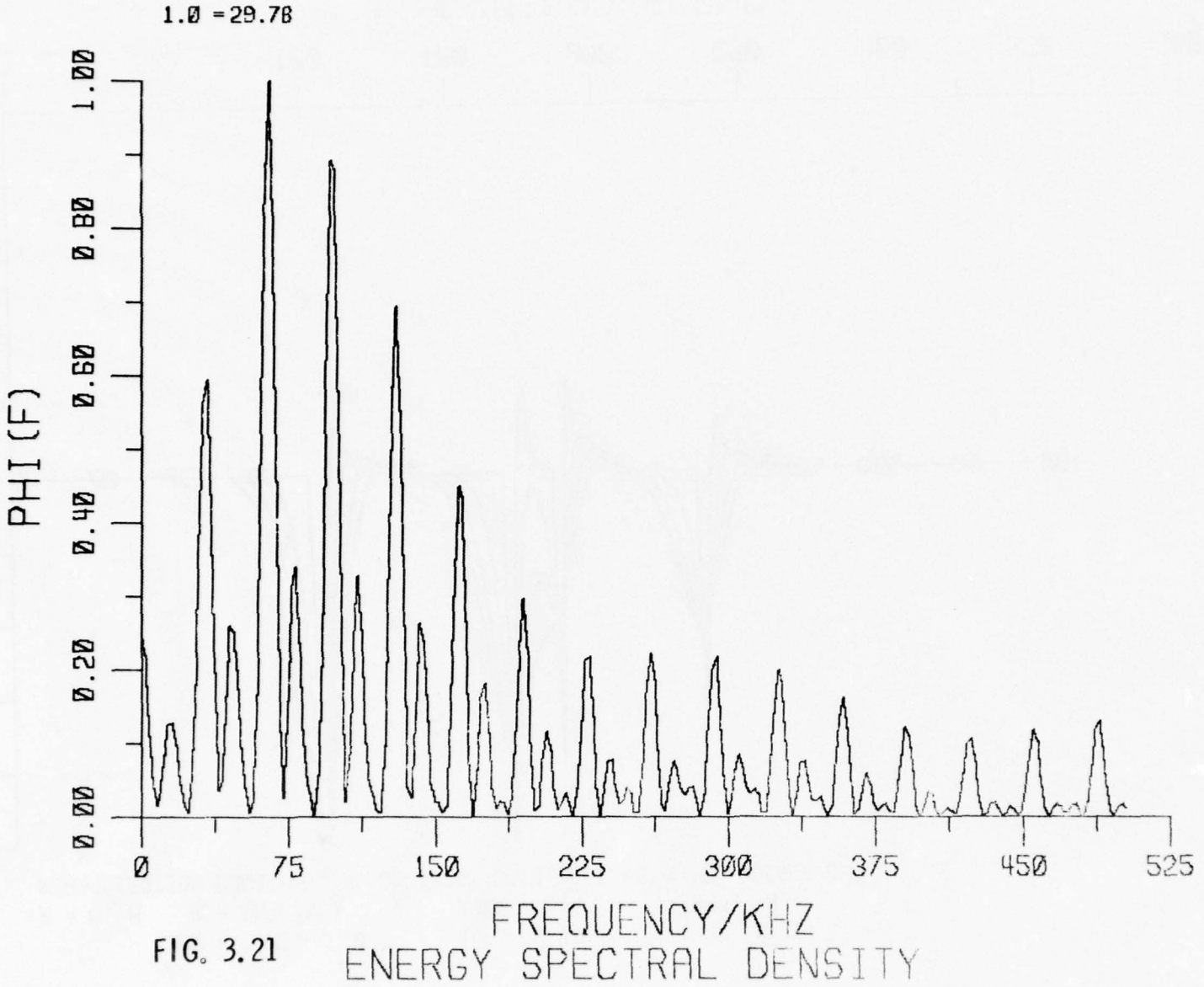
1.0 =29.78
PHI(F)
0.00
0.20
0.40
0.60
0.80
1.00
0
75
150
225
300
375
450
525
FREQUENCY/KHZ
ENERGY SPECTRAL DENSITY

FIG. 3.21

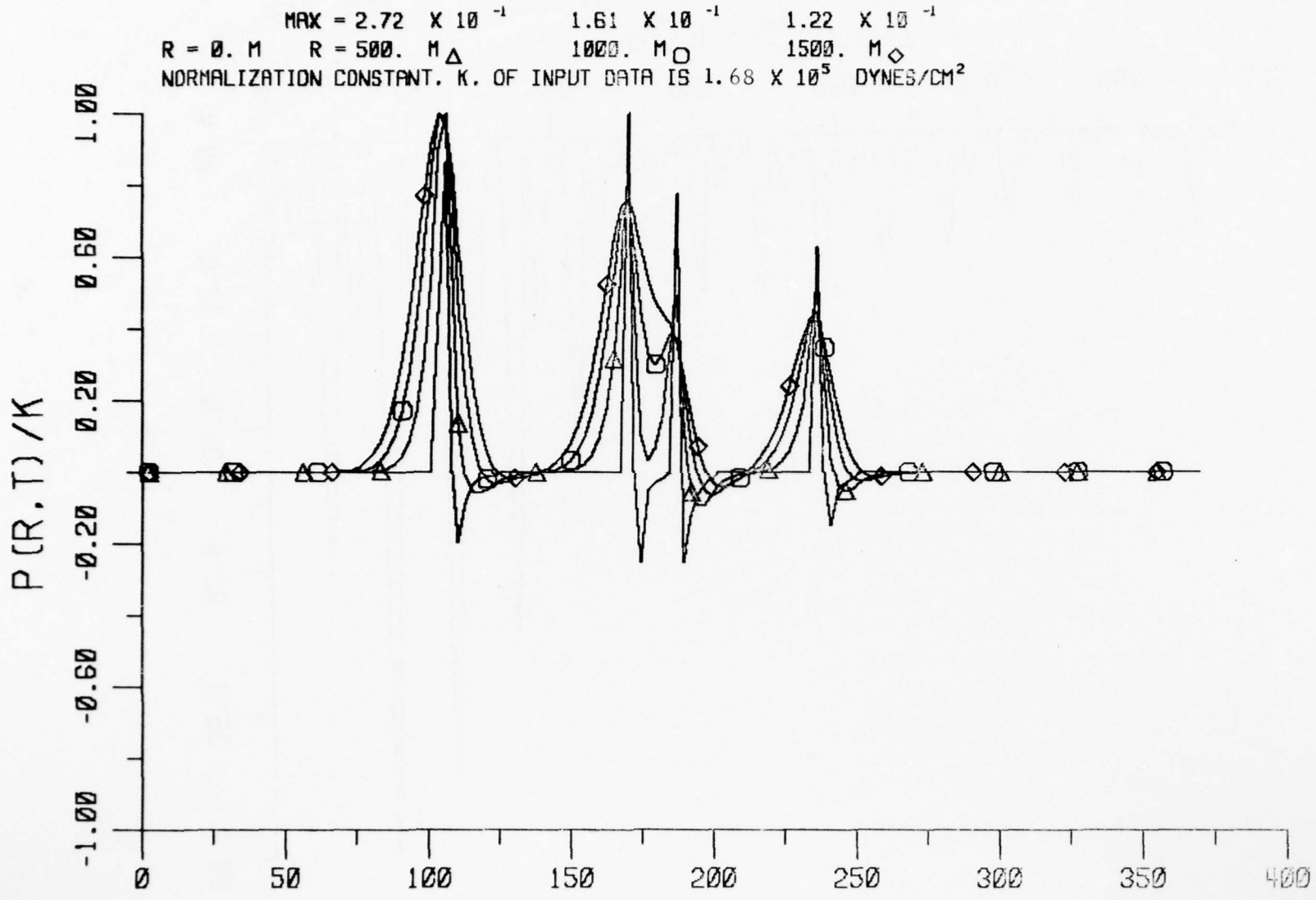

FIG. 3.22 ACOUSTIC SIGNATURES

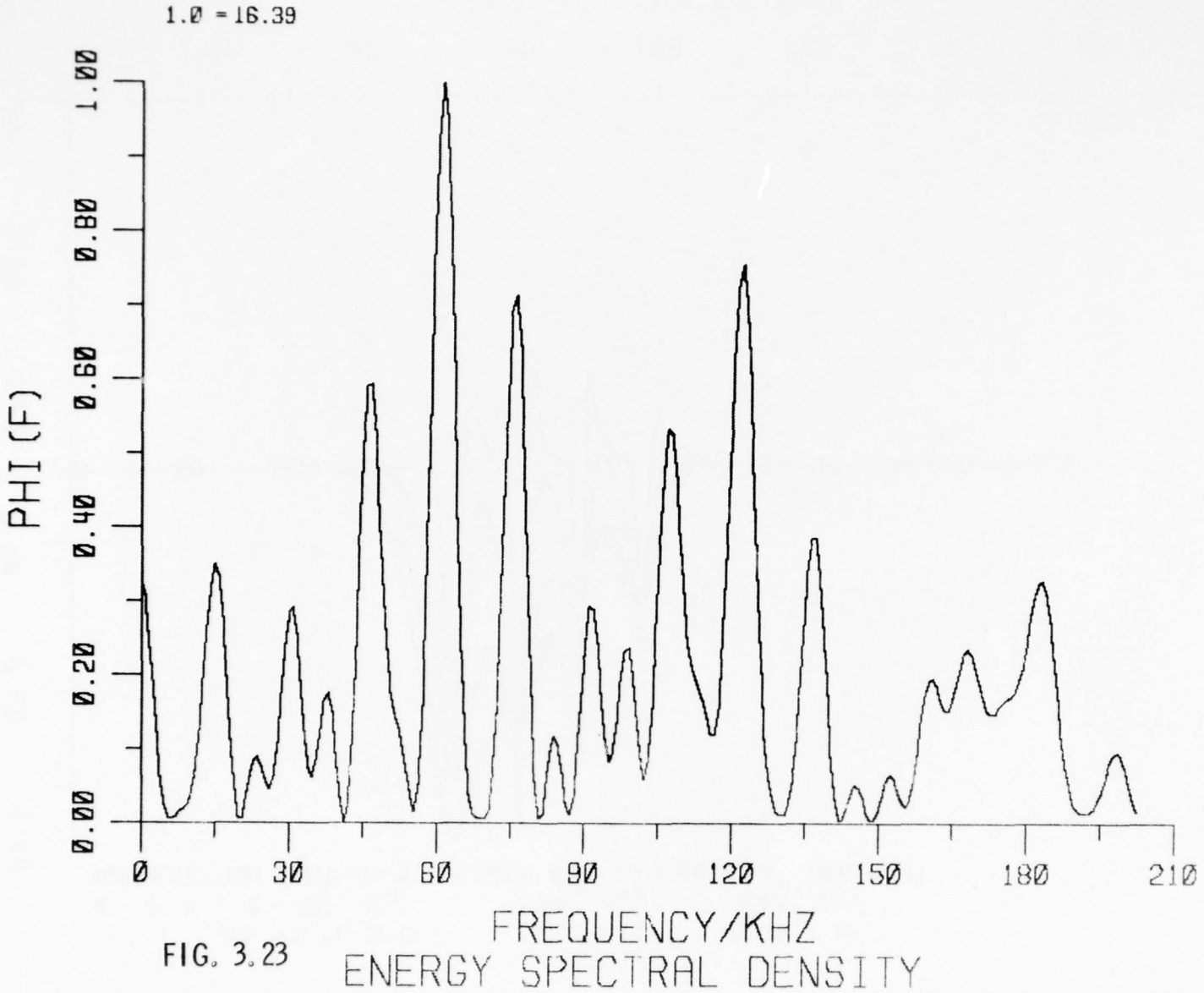
1.0 = 16.39
PHI(F)
0.00
0.20
0.40
0.60
0.80
1.00
0
30
60
90
120
150
180
210
FREQUENCY/KHZ
ENERGY SPECTRAL DENSITY

FIG. 3.23

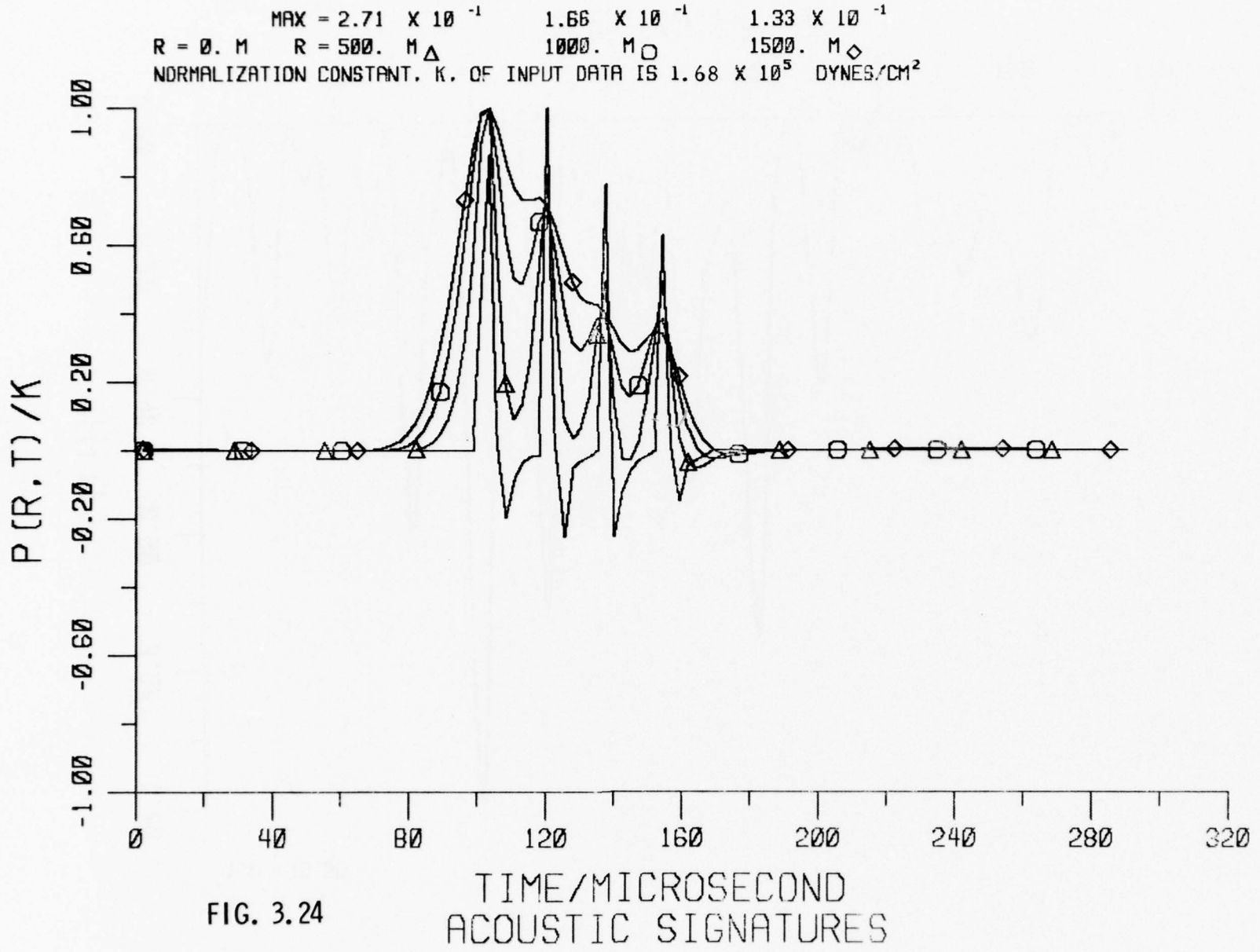

FIG. 3.24

ACOUSTIC SIGNATURES

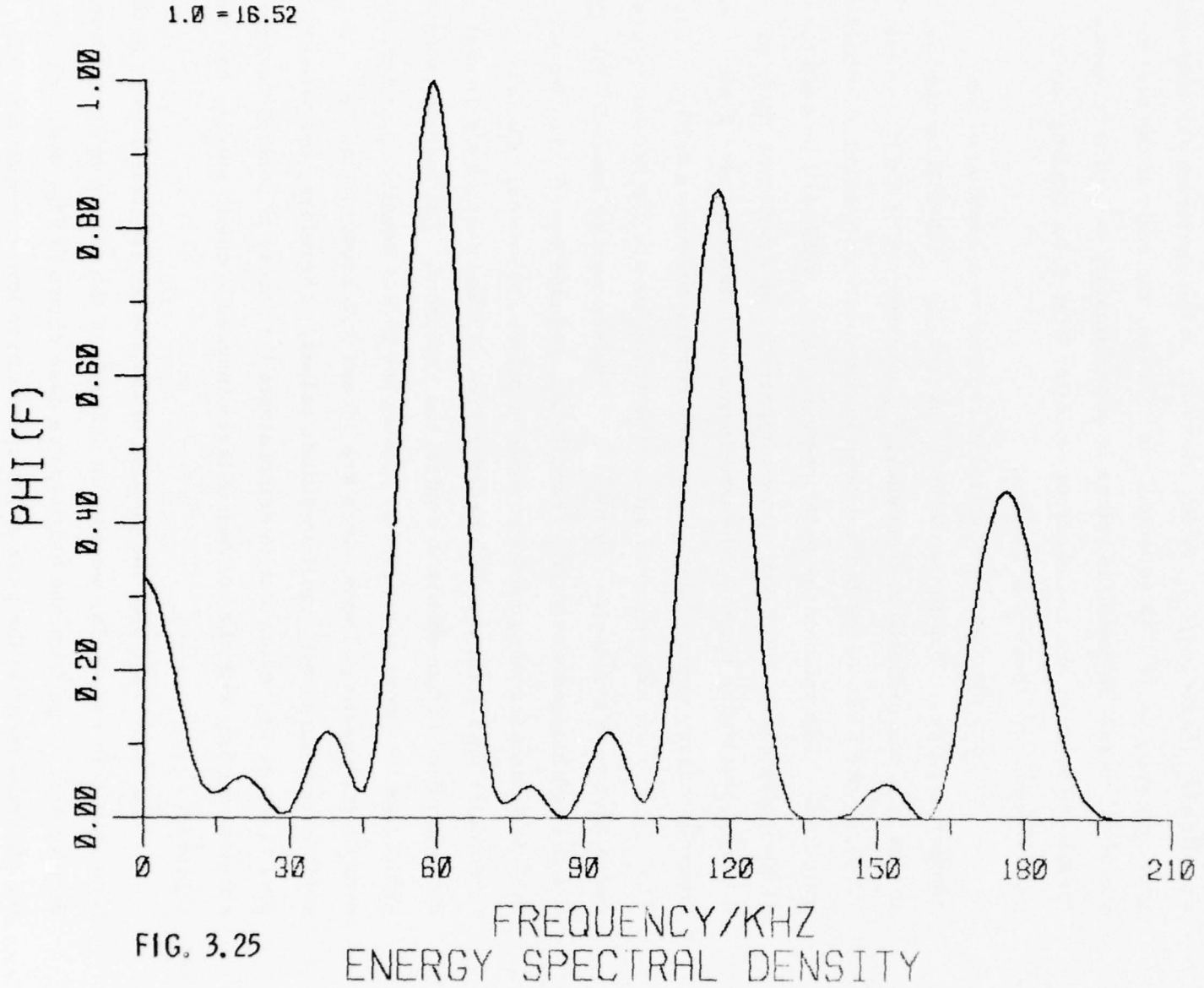
1.0 = 16.52
PHI(F)
0.00
0.20
0.40
0.60
0.80
1.00
0
30
60
90
120
150
180
210
FREQUENCY/KHZ
ENERGY SPECTRAL DENSITY

FIG. 3.25

Figs. 3.26 to 3.33, and the characteristic modulations of approximately $\sin^2 (N\pi f/f_o)/\sin^2 (\pi f/f_o)$. Also, the peaks in the spectrum are increasing approximately as N^2, as expected. In addition, the ratio of the peak to the small bumps between the spikes is approximately N^2. These waveforms and spectra are analogous to those for Fig. 2.8. Scaling can be established from these calculations.

We now discuss the spectral narrowing as a function of the number of pulses. The measure of the narrowing which will be used is the ratio of the modulation frequency, f_o, (the inverse of the interpulse time), to the width of the highest peak in the spectrum measured at half amplitude. The ratio of the peak frequency to the width will be used for the single-pulse cases which will allow comparisons of waveforms made at different interpulse times. The waveforms described in Table 2 were analyzed from the energy spectral densities. The results are shown in Fig. 3.34. The O's are the experimental data. The triangles are the two four pulse cases that were synthesized by making the pulses equally spaced. The □'s are the synthesized waveforms from the single-pulse waveform. We see the spectrum narrowing as the number of pulses increases. The best three pulse data point was 28% broader than an ideal case, a significant demonstration of our ability to control the spectrum. The four-pulse data signatures that were corrected by making the pulses equally spaced exhibit even better results. These cases are 3% and 13% broader than the synthesized signal with equal amplitude pulses. Therefore, the primary goal of the study, which was to demonstrate the ability to control the energy spectral density with the number of laser induced acoustic pulses, has been achieved.

We have restricted the plotting of the energy spectral density to the input data. In Fig. 3.35, we give an example of the change in energy spectral density with range from the single-pulse case shown in Fig. 3.4. We note the expected trend in the peak of the spectrum to lower frequencies for greater propagation distances.

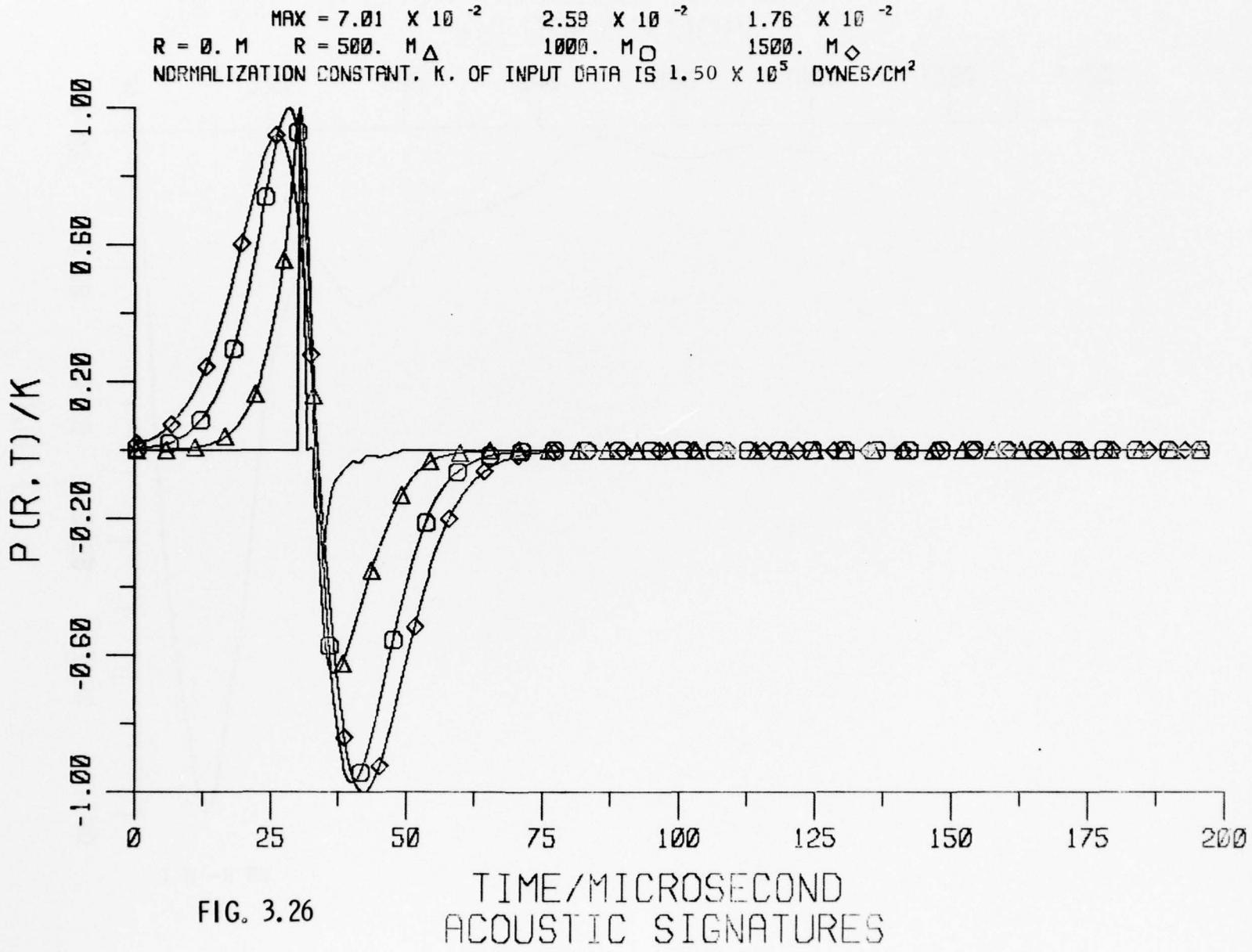
MAX = 7.01 X 10 -2
2.59 X 10 -2
1.76 X 10 -2
R = 0. M
R = 500. M Δ
1000. M ○
1500. M ◇
NORMALIZATION CONSTANT, K, OF INPUT DATA IS 1.50 X 10^5 DYNES/CM^2
P(R,T)/K
1.00
0.60
0.20
-0.20
-0.60
-1.00
0
25
50
75
100
125
150
175
200
TIME/MICROSECOND
ACOUSTIC SIGNATURES

FIG. 3.26

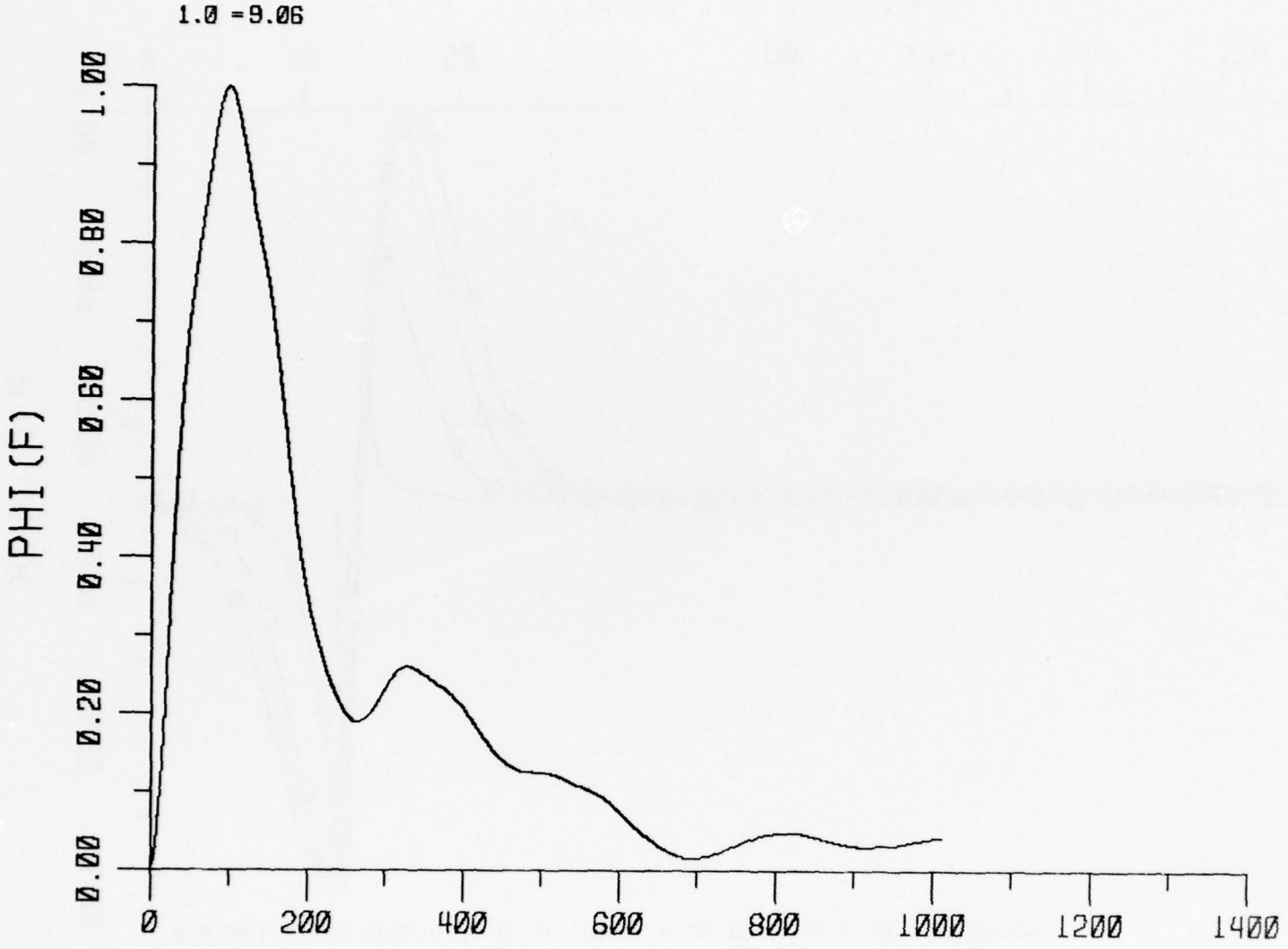
1.0 =9.06
PHI(F)
0.00
0.20
0.40
0.60
0.80
1.00
0
200
400
600
800
1000
1200
1400
FREQUENCY/KHZ
ENERGY SPECTRAL DENSITY

FIG. 3.27

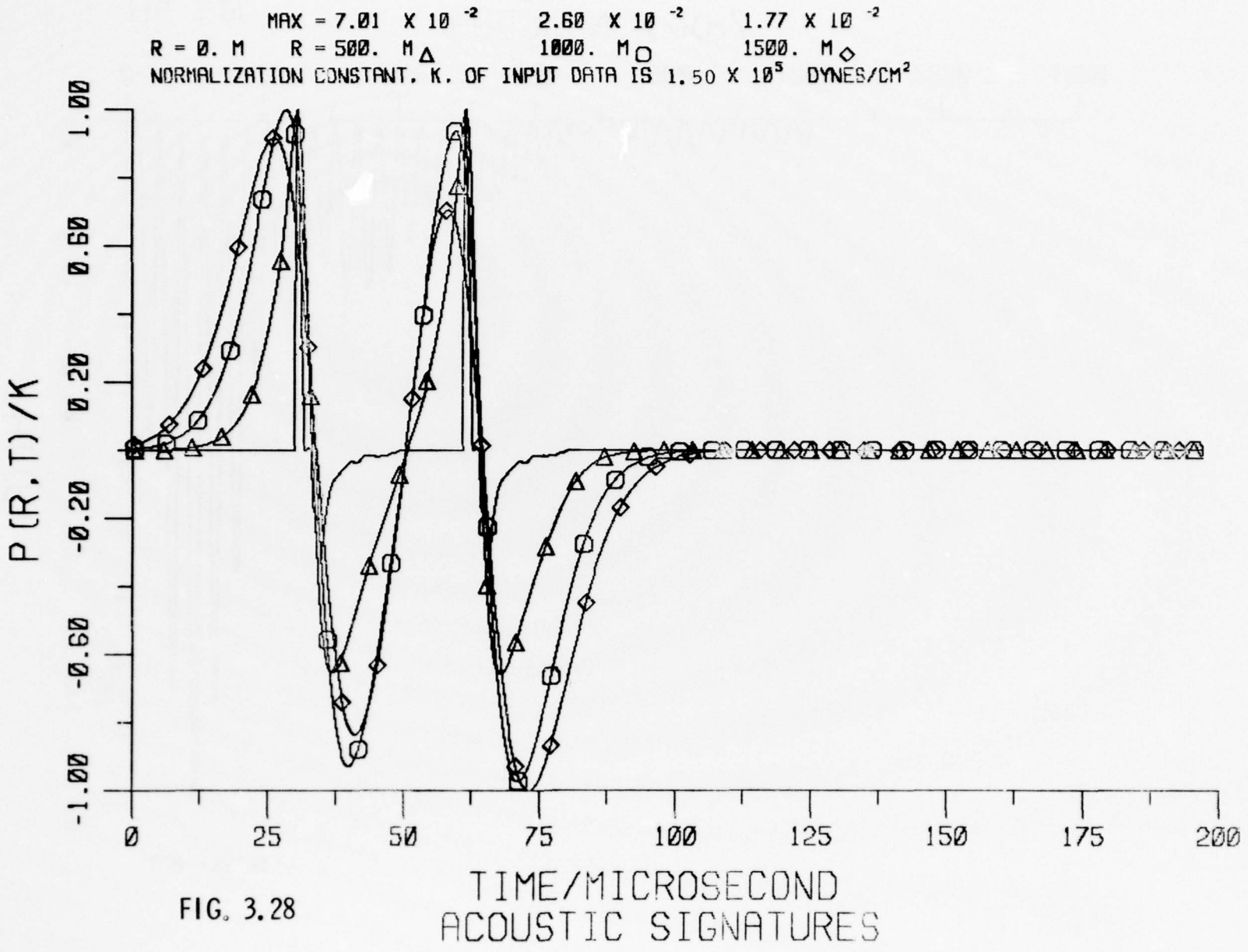

FIG. 3.28

ACOUSTIC SIGNATURES

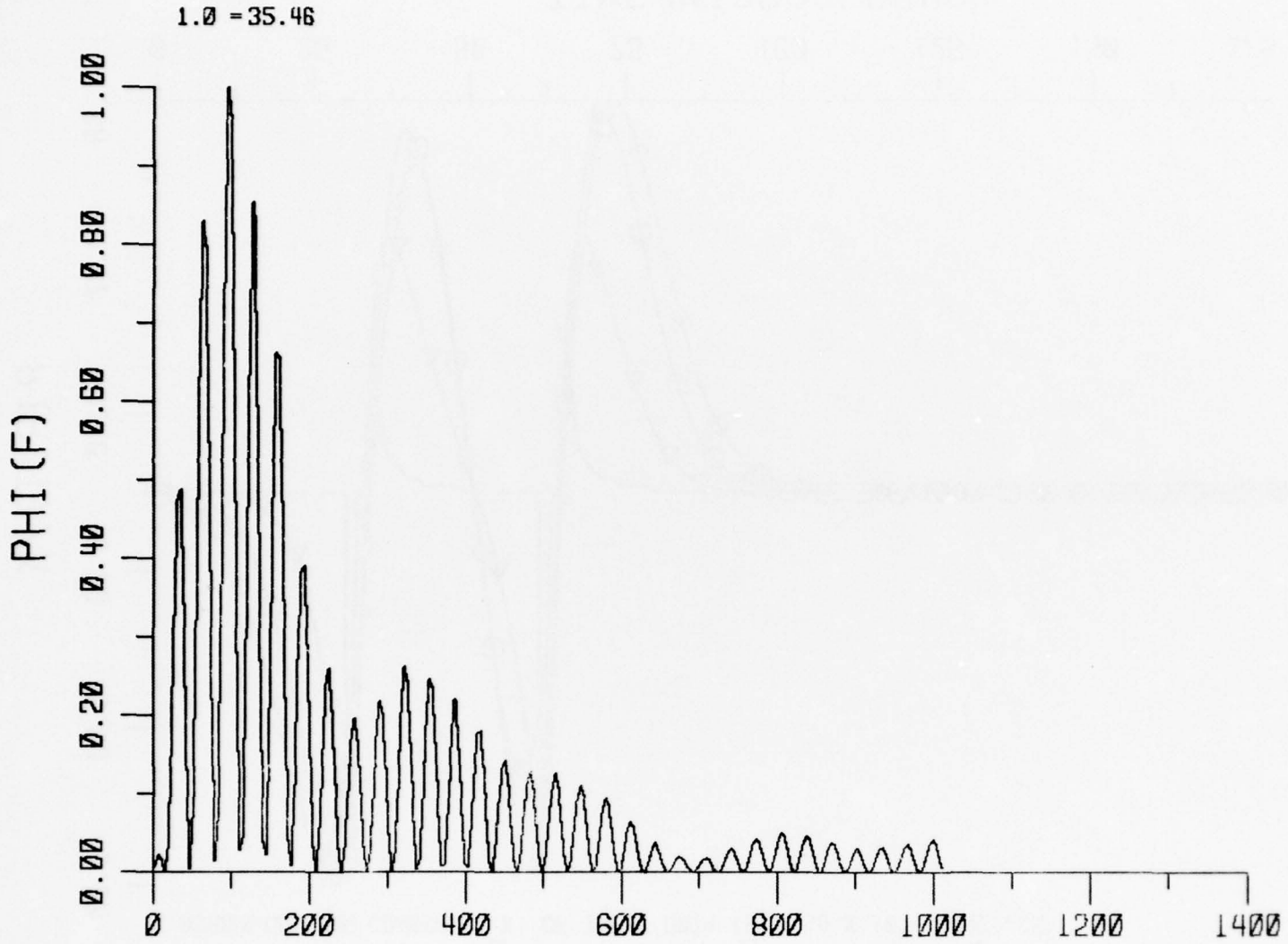
1.0 =35.46
PHI(F)
0.00
0.20
0.40
0.60
0.80
1.00
0
200
400
600
800
1000
1200
1400
FREQUENCY/KHZ
ENERGY SPECTRAL DENSITY

FIG. 3.29

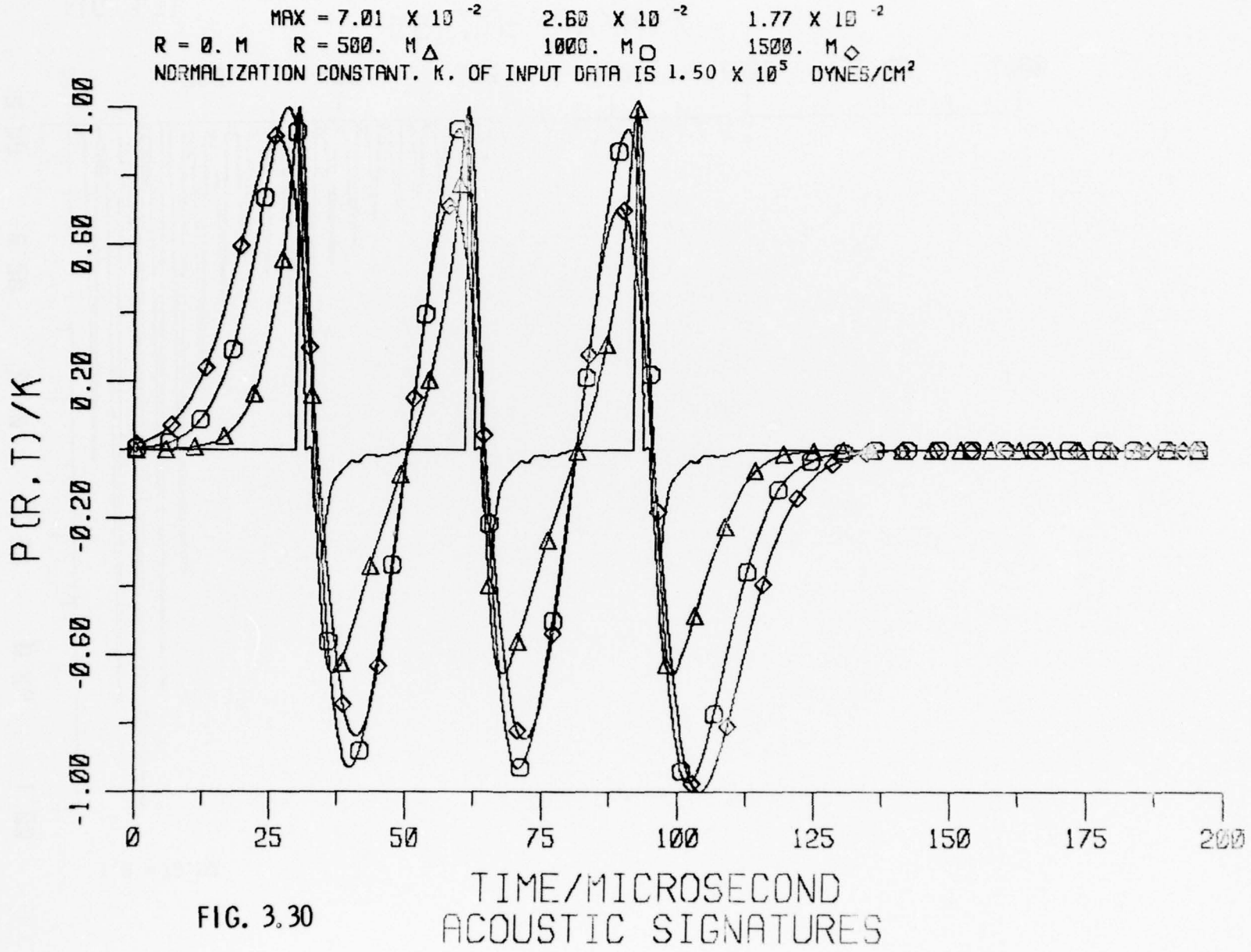

FIG. 3.30 ACOUSTIC SIGNATURES

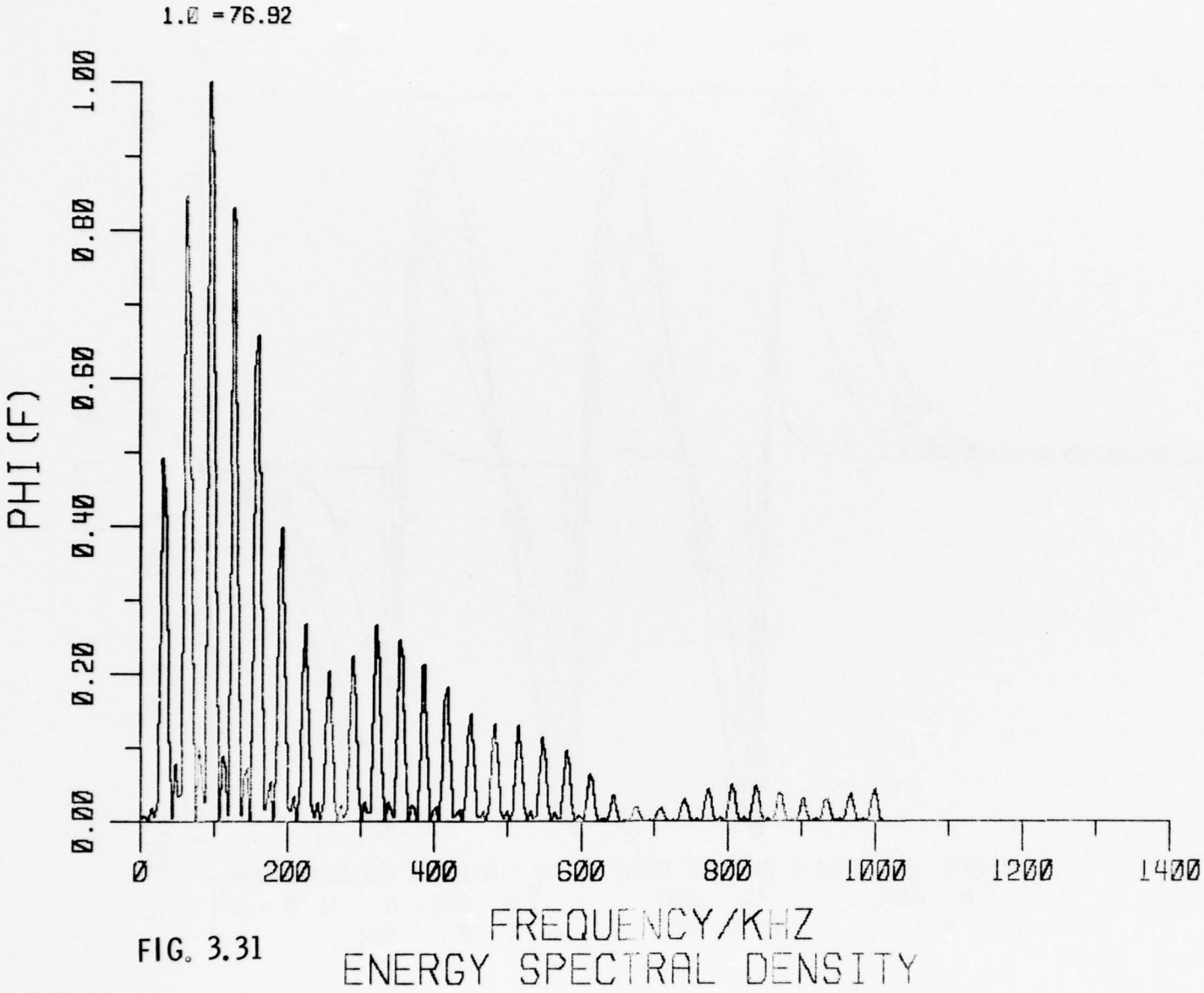
1.0 =76.92
PHI(F)
0.00
0.20
0.40
0.60
0.80
1.00
0
200
400
600
800
1000
1200
1400
FREQUENCY/KHZ
ENERGY SPECTRAL DENSITY

FIG. 3.31

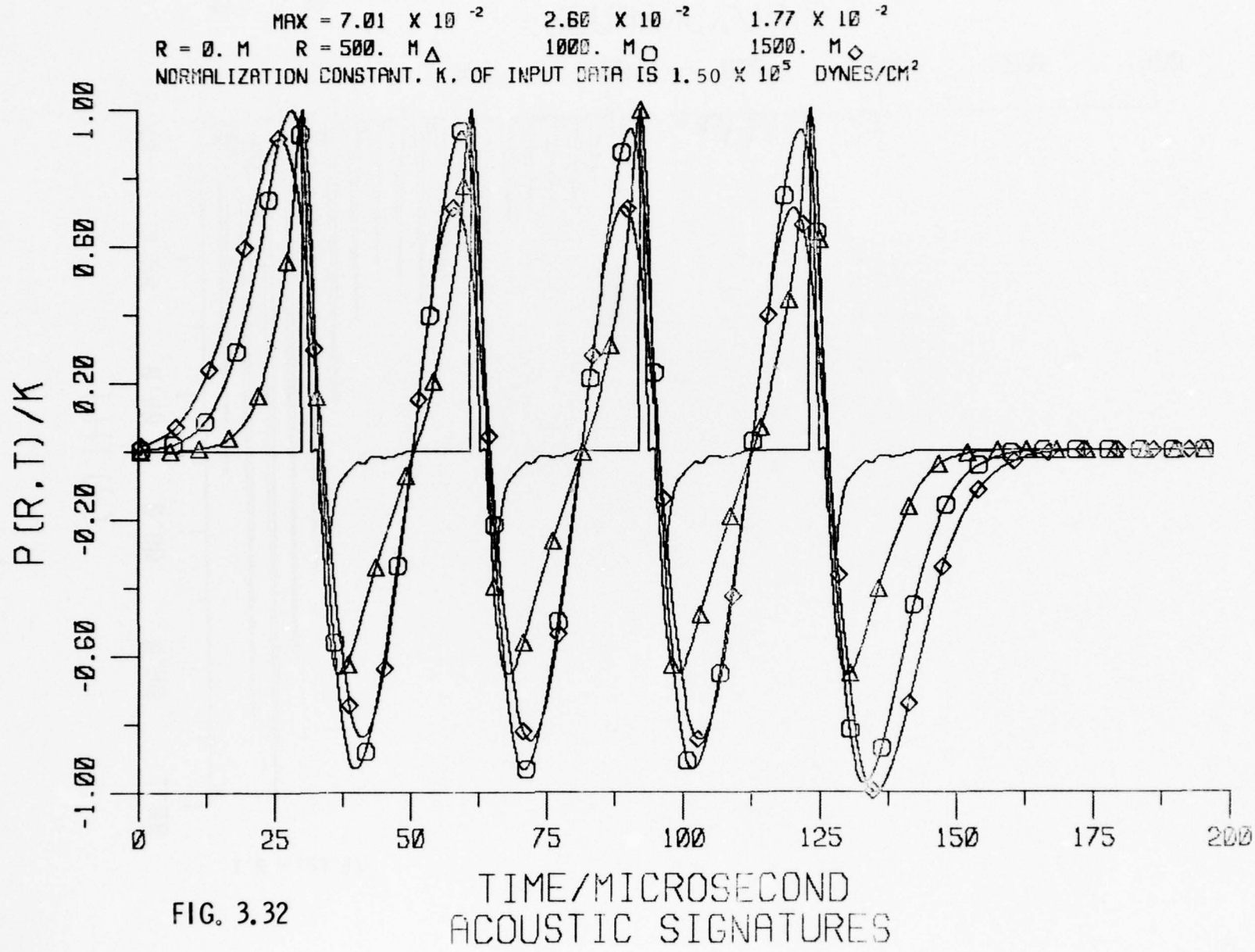
MAX = 7.01 X 10 -2
2.60 X 10 -2
1.77 X 10 -2
R = 0. M
R = 500. M
1000. M
1500. M
NORMALIZATION CONSTANT. K. OF INPUT DATA IS 1.50 X 10^5 DYNES/CM^2
P(R,T)/K
1.00
0.60
0.20
-0.20
-0.60
-1.00
0
25
50
75
100
125
150
175
200
TIME/MICROSECOND
ACOUSTIC SIGNATURES

FIG. 3.32

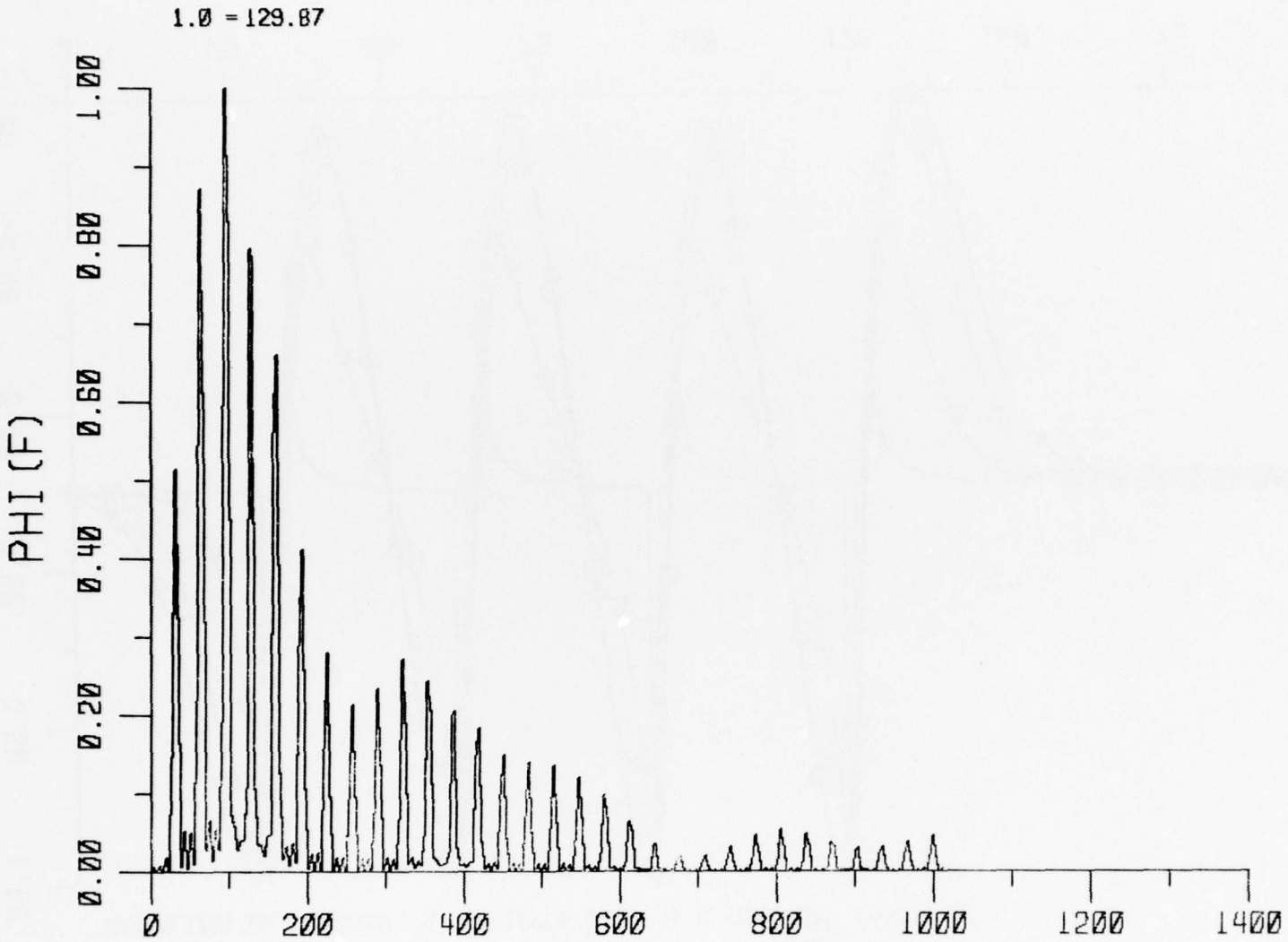
1.0 = 129.87
PHI(F)
0.00
0.20
0.40
0.60
0.80
1.00
0
200
400
600
800
1000
1200
1400
FREQUENCY/KHZ
ENERGY SPECTRAL DENSITY

FIG. 3.33

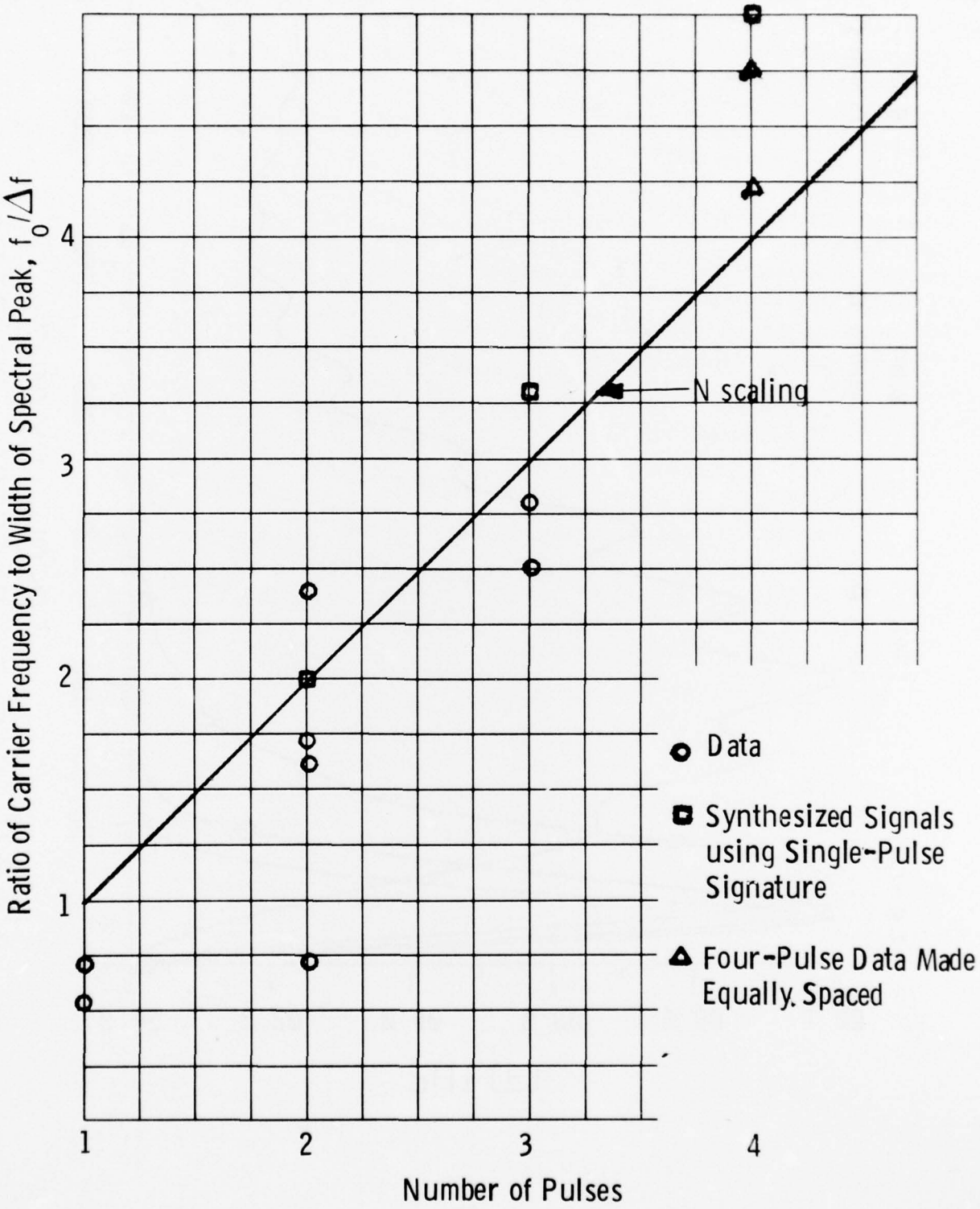

Fig. 3.34 Spectral Narrowing Vs. Number of Pulses

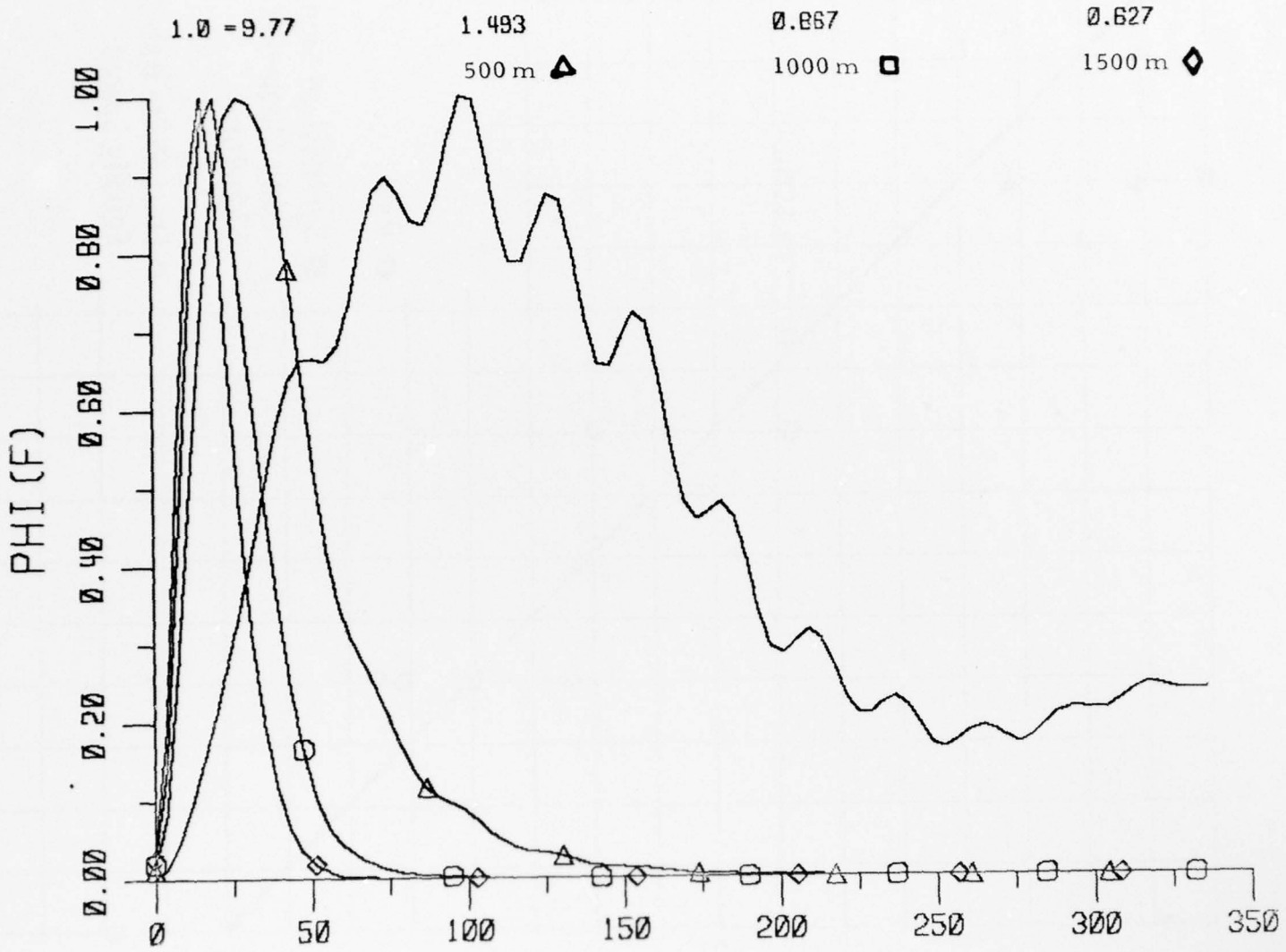
1.0 =9.77
1.493
500 m
0.867
1000 m
0.627
1500 m
PHI(F)
0.00
0.20
0.40
0.60
0.80
1.00
0
50
100
150
200
250
300
350
FREQUENCY/KHZ
ENERGY SPECTRAL DENSITY

FIG. 3.35

IV. SUMMARY AND SUGGESTIONS FOR FUTURE WORK

The basic experimental goal of the study, the ability to control the energy spectral density of a laser-induced acoustic signature, was accomplished. Specifically, it has been demonstrated that as the number of evenly spaced laser pulses increased, the width of the fundamental or harmonic peak in the spectrum is decreased. The theoretical performance was not achieved because the laser-induced pulses were not identical in amplitude, shape, and interpulse time. However, an experimentally obtained three-pulse signature was analyzed in detail, and it was found that the spectrum was only 1.28 times as broad as the theoretical value. Because there is only a small difference between the theoretical width and the experimental width, the basic objective of the experiments has been achieved.

The secondary goal of the experiments was to obtain signatures which did not have even interpulse times, so that the spectrum would remain broad. It is not possible to fully demonstrate this concept with only four pulses, but it was demonstrated that the resulting spectrum was much broader than one with four evenly spaced pulses.

The experiments discussed in this report have demonstrated the concept of spectral narrowing of laser-induced acoustic signatures. Quantitative experiments are yet to be done to verify several scientific issues. First, the efficiency of converting laser energy to useful acoustic energy should be experimentally determined. A modest theoretical effort, using the existing models to estimate conversion efficiencies as a function of needed acoustic signatures, should be carried out. The relationship between laser parameters, breakdown level, and the resulting acoustic signature remains to be established. Finally, the optimum IR laser wavelength to maximize the conversion efficiency should be demonstrated.

Second, comprehensive experiments need to be done to quantitatively validate the relationship between the various laser parameters (i.e. number of pulses, energy, interpulse time, etc.) and the resulting signature parameters, i.e. amplitude and spectrum.

Third, the acoustic radiation pattern needs to be studied because many applications would utilize the acoustic radiation at shallow angles. Because of the broadband nature of the source, the signature and radiation pattern will be dependent on source size and laser parameters. Both the ideal angular dependence, on a flat surface, and the nonideal case of a wavy surface require experimental and theoretical investigation.

After the above issues have been addressed, the needs of numerous applications can be matched with capabilities. A limited systems study has already been carried out to establish some specific needs.[6]

REFERENCES

1. F. N. Bunkin, N. V. Karlov, V. M. Komissarov, and G. P. Kuz'min, JETP Lett. 13, 341 - 3 (1971).

2. P. E. Nebolsine and R. F. Weiss, "Radiation Induced Sound" (U), Avco Everett Research Laboratory, Document No. 73-729 (June 1, 1973) - Confidential.

3. R. G. Cawley and C. E. Bell, "Propagation of CO_2 Laser (10.6 μ Induced Pressure Transients in Water (U)", NOLTR 72-207 (17 Sept. 1972) - Confidential.

4. P. E. Nebolsine, "Radiation Induced Sound Field Demonstration Program" (U), Avco Everett Research Laboratory, Document 74-154 (February 1974) - Confidential.

5. B. S. Maccabee and C. E. Bell, "Properties of Laser Induced Sound in the Ocean" (U), Naval Ordnance Laboratory, November 1973 - Confidential.

6. P. E. Nebolsine, "Thermoacoustics" PSI TR-12, August 15, 1974 (Confidential).

7. J. I. Bowen and P. E. Nebolsine, "An Underwater Application of Optically Induced Sound" (U), Raff Rpt. 75-8, July 1975 (Secret).

8. C. E. Bell and B. S. Maccabee, "Shock Wave Generation in Air and in Water by CO_2 TEA Laser Radiation, Applied Optics 13, 605-609 (1974).

9. P. E. Nebolsine, P.K.S. Wu and L. N. Myrabo, "Laser Impulse Applications Research" (U), PSI TR-75, January 1977 - Secret.

10. E. K. Dabora, "Variable Energy Blast Waves", AIAA J. 10, 1384-1386 (1972).

11. R. E. Schlier, A. N. Pirri, D. J. Reilly, "Air Breakdown Studies, AFWL TR-72-74, February 1973.

12. R. J. Urick, Principles of Underwater Sound for Engineers, McGraw-Hill, New York, 1967.

13. C. W. Horton, Sr., "Dispersion Relationships in Sediments and Seawater", J. Acous. Soc. Am. 55, 547 (1974).

DISTRIBUTION FOR

FINAL REPORT

CONTRACT # N00014-76-C-0693

	Copies
Defense Documentation Center Cameron Station Alexandria, Virginia 22314	12
Director Naval Research Laboratory Code 2627 4555 Overlook Avenue S. W. Washington, D. C. 20375	6
Office of Naval Research Code 222 800 N. Quincy Street Arlington, Virginia 22217	12
Office of Naval Research Branch Office 495 Summer Street Boston, Massachusetts 02210	1
Commander Naval Sea Systems Comm Department of the Navy Washington, D. C. 20362 Attn: Code 06H1	1
Commander Naval Sea Systems Comm Department of the Navy Washington, D. C. 20362 Attn: 06H2	1
Commander Naval Electronic Sys. Comm. Code 320 2511 Jefferson Davis Hgwy. National Center #1 Arlington, Virginia 20360	1
Commander Naval Electronic Sys. Comm. PME 124-40 2511 Jefferson Davis Hgwy. National Center #1 Arlington, Virginia 20360	1
Commanding Officer Naval Underwater Sys. Ctr. New London Laboratory New London, Conn. 06320	1
Commanding Officer Naval Ocean Res. & Develop. Activity NSTL Station Mississippi 39529	2
Chief of Naval Material NAVMAT 03T Dept. of the Navy Washington, D. C. 20360	2
John Hopkins University Applied Physics Lab. SSBN Security Program Johns Hopkins Road Laurel, Maryland 20810	1
Raytheon Corporation Submarine Signal Div. Portsmouth, R. I. 02871	1
Edo Corporation 1310 11th Street College Point, N. Y. 11356	1
Prof. O. M. Baycura Naval Postgrad. School Monterey, California 93940	1